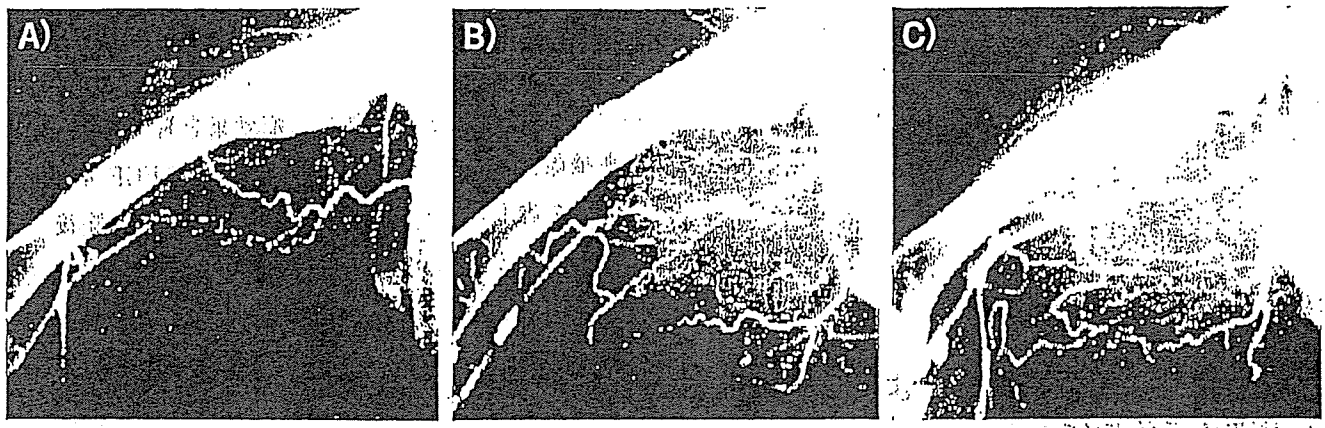

○図３　下肢虚血モデル家兎の遺伝子治療後38日目における新生血管
家兎虚血肢モデルの血管造影においてコントロール例（A）に比較して，FGF-4遺伝子投与群（BおよびC）において有意な新生血管の増加を認めた

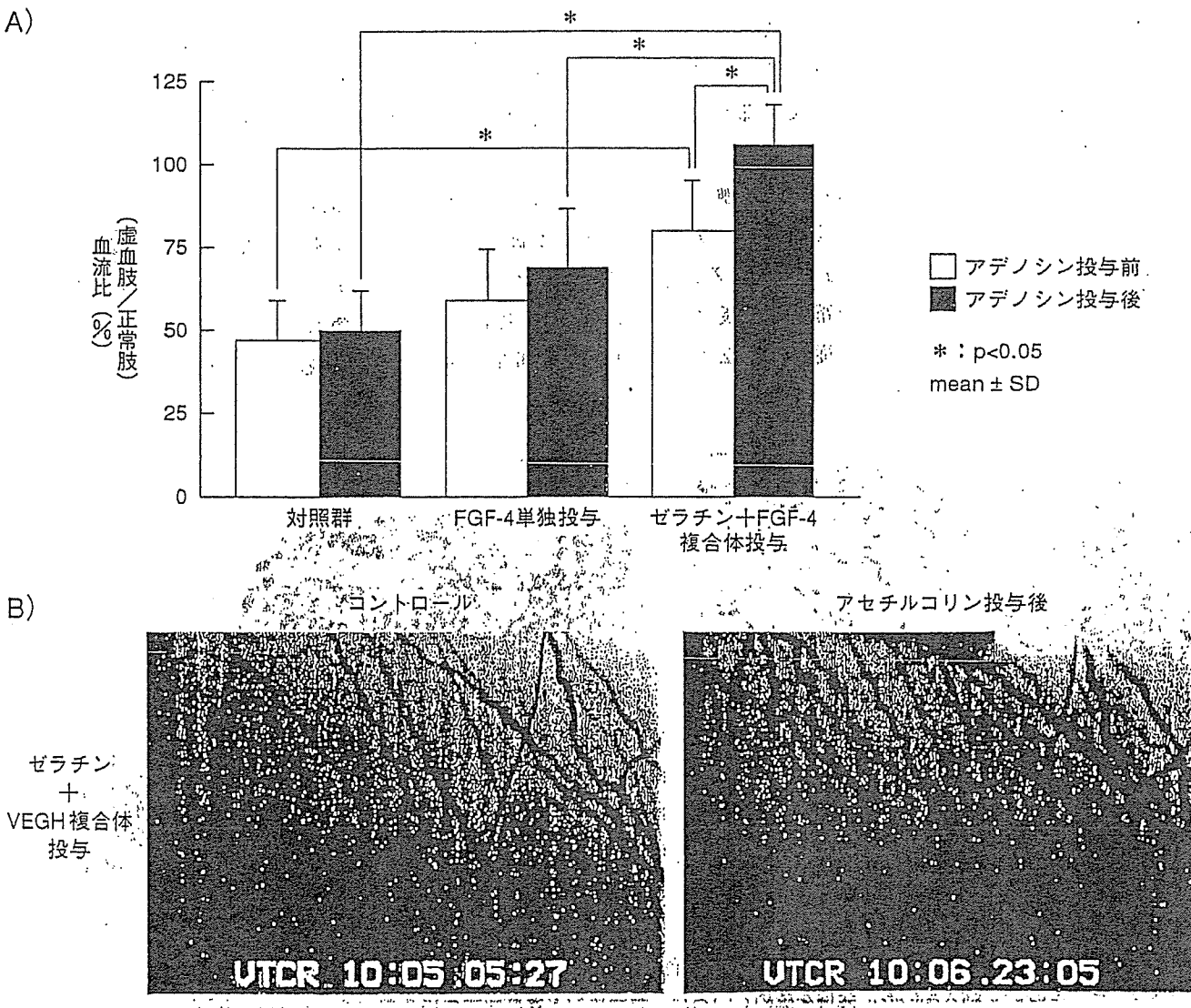

○図４　A）下肢虚血モデルに対する遺伝子治療の効果とアデノシンに対する反応性（マイクロスフェアー法による）．B）アセチルコリンに対する新生血管の反応性（放射光微小血管造影法）

遺伝子治療汎用化への展望

1. 現行の遺伝子治療に求められる改良点

VEGFやbFGFの組換えタンパクあるいはプラスミドDNA・ウイルスベクターを用いた組換え遺伝子の投与による血管新生療法には問題や限界がある．VEGFを例にとると，虚血部位での周皮細胞の不足した未成熟な新生血管が発生し，結果として易出血性を示し，透過性亢進による浮腫が生じやすくなってしまう．そうした問題に対してBlauらは，調和のとれた再生血管床を得るために以下の3つの概念を述べている[12]．

①持続期間を調節する機能をもったベクターとともに投与して，至適な量と持続時間で血管成長因子が作用するようにする．

②内皮細胞を安定化させるアンジオポエチン-1や周皮細胞を動員するPDGF-BB等補充的な効果をもつ調節因子を血管成長因子とともに投与する．

③虚血時に分泌される血管成長因子，PDGF-BB，アンジオポエチン-2を血管内皮細胞から分泌させるHIF-1αのような多面発現性をもった因子を投与する．または，HIF-1αの代謝を抑制するPR39といったさらに上流の調節因子を投与することによって，最終的にはバランスのとれた複数の調節因子を作用させる．

2. 細胞を基地とした遺伝子治療 (Cell-based gene therapy)

遺伝子または調節因子の投与のみでは代謝による影響があり，必要とされる局所への有効量の到達の面で限界がある．目的としている臓器にある細胞の中に遺伝子を発現させてから投与し，細胞内での持続的遺伝子産生によって長期的に局所に遺伝子を発現させる方法がCell-based gene therapyである．血管においては内皮細胞・平滑筋細胞・線維芽細胞，心筋においては骨格筋筋芽細胞等が用いられ，細胞投与後2週間以上の遺伝子発現持続が認められ良好な効果が得られている[13]．

3. 細胞/遺伝子ハイブリッド型治療 (Cell/Gene Hybrid therapy)

Cell-based gene therapyでは細胞は遺伝子発現の元としての機能しか果たしていない．われわれはBlauらの主張をふまえて，今後の遺伝子治療としてCell/Gene Hybrid-therapyという概念を提案する．

最近の血管新生療法においては，骨髄単核球や血管内皮前駆細胞を経管的に移植する方法が試みられており，細胞移植による血管新生療法の可能性が示唆されている．これらの細胞移植の長所に加えて細胞内で遺伝子を発現させることによって，細胞と遺伝子の相乗作用で血管床を再生するという概念がハイブリッド遺伝子治療法である．われわれは生分解性ゼラチンを用いた細胞内遺伝子導入法を考案した．貪食能をもつ細胞（マクロファージや血管内皮前駆細胞）は遺伝子を吸着させたゼラチンを高率に貪食するため，細胞内への導入が可能となる（図5）．走化性をもつマクロファージや単球に血管成長因子の遺伝子を導入し，この細胞を経管的に投与して血管再生治療を行う．これらの細胞は傷害部位に特異的に集まるために，局所の遺伝子発現効率が高まる．しかも，線維芽細胞や平滑筋細胞と異なり血管内へ投与しても凝集することがなく，血管内投与が可能となる．

さらに，血管内皮前駆細胞の有するvasculogenesis, angiogenesisと補完的な作用を有する遺伝子を導入することで，より成熟した血管床を再構築することを目指しており，本法の難治性の循環障害（心筋梗

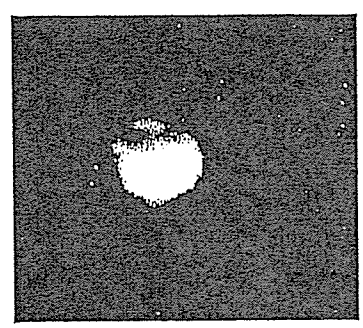

○図5　ゼラチン-GFPを貪食しGFPが細胞質内で発現しているマウス・マクロファージ

塞，下肢虚血，原発性肺高血圧症等）の治療への適応を検討中である．血管発生能を有する血管内皮前駆細胞に強い血管拡張作用を有するアドレノメジュリンを組合せることにより，毛細血管再生にとどまらず，上流にあたる細小動脈のリモデリングを含めた総包括的な血管再生が期待されている．

これからの基礎医学研究に望むこと

循環器領域における遺伝子治療，再生医療が，初期からその有効性が報告され臨床応用が進んでいるなかで，遺伝子治療としての臨床応用はわが国としては米国に大きく後れをとっている．しかし，近年，骨髄単核球投与による血管新生療法が世界に先駆けての臨床応用が開始され，その有効性が報告されている．

臓器レベルの循環障害を血管再生医療で克服するには安全性と有用性の両面で一層の基礎医学における進歩が求められている．作用を患部にとどめること，そして十分に機能的な血管系の再構築が求められており，細胞機能の強化を図るハイブリッド治療が必要部位に限局したより大きな効果を生むものとして，新たな遺伝子治療の展開をみせていくものとして期待される．

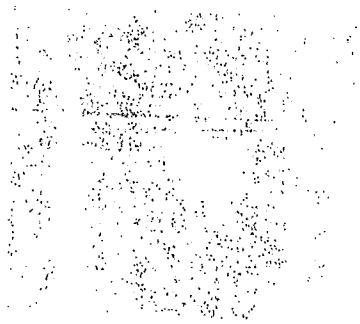

文　献

1) Folkman, J. : n Engl. J. Med., 285 : 1182-1186, 1971
2) Hockel, M. et al. : Arch. Surg., 128 : 423-429, 1993
3) Isner, J. M. et al. : Lancet, 348 : 370-374, 1996
4) Cindy, L. G. et al. : Circulation, 105 : 1291-1297, 2002
5) Soker, S. et al. : Cell, 92 : 735-745, 1998
6) Nakamura, Y. et al. : J. Hypertens., 14 : 1067-1072, 1996
7) Igarashi, R. et al. : J. Controlled Release, 71 : 157-164, 2001
8) Koch, A. E. et al. : Science, 258 : 1798-1801, 1992
9) Fajardo, F. L. et al. : Am. J. Pathol., 140 : 539-544, 1992
10) Takakura, N. et al. : Cell, 102 : 199-209, 2000
11) Tateishi-Yuyama, E. et al. : Lancet, 360 : 427-435, 2002
12) Blau, H. M. et al. : Nature Med., 7 : 532-534, 2001
13) Suzuki, K. et al. : Circulation, 104 [Suppl I] : I 207-I 212, 2001

●筆頭著者プロフィール●

國本 聡：1989年日本大学医学部卒業，'95年日本大学大学院卒業，'96年から'98年まで米国ノースカロライナ大学循環器科に留学，Leonard S. Gettes教授のもと虚血性心疾患に伴う致死的不整脈の原因について研究．帰国後，虚血性疾患の遺伝子治療の研究に従事し，東海大学医学部生理科学教室浅原孝之教授のもとで血管内皮前駆細胞について研究指導を受けた後，現在国立循環器病センター研究所においてさらなる展開を目指して研究中．

tapraid4/zh8-bloo/zh8-bloo/zh800407/zh80803d07g | sangreyj | S=4 | 12/9/06 | 19:57 | Art: 2006/029298 | Input-DCT-???

Collection Codes: 11

DOI: 10.1182/blood-2006-06-029298
HEMOSTASIS, THROMBOSIS, AND VASCULAR BIOLOGY

Receptor activator of nuclear factor (NF)–κB ligand (RANKL) increases vascular permeability: impaired permeability and angiogenesis in eNOS-deficient mice

AQ: 0

Jeong-Ki Min, Young-Lai Cho, Jae-Hoon Choi, Yonghak Kim, Jeong Hun Kim, Young Suk Yu, Jaerang Rho, Naoki Mochizuki, Young-Myeong Kim, Goo Taeg Oh, and Young-Guen Kwon

[1]Department of Biochemistry, College of Sciences, Yonsei University, Seoul, Republic of Korea; [2]Department of Molecular and Cellular Biochemistry, School of Medicine, Kangwon National University, Chunchon, Kangwon-Do, Republic of Korea; [3]Department of Ophthalmology, Seoul National University College of Medicine, Seoul National University Hospital, Seoul, Republic of Korea; [4]Seoul Artificial Eye Center, Clinical Research Institute, Seoul National University Hospital, Republic of Korea; [5]Department of Structural Analysis, National Cardiovascular Center Research Institute, Osaka, Japan; [6]Department of Microbiology, College of Natural Sciences, Chungnam National University, Daejeon, Republic of Korea; [7]Division of Molecular Life Science, Ewha Womans University, Seoul, Republic of Korea

Receptor activator of nuclear factor (NF)–κB ligand (RANKL) is emerging as an important regulator of vascular pathophysiology. Here, we demonstrate a novel role of RANKL as a vascular permeability factor and a critical role of endothelial nitric oxide synthase (eNOS) in RANKL-induced endothelial function. RANKL increased the vascular permeability and leukocyte infiltration in vivo and caused the breakdown of the blood-retinal barrier in wild-type mice but not in eNOS-deficient mice. In vitro, it increased endothelial permeability and reduced VE-cadherin–facilitated endothelial cell-cell junctions in a NO-dependent manner. RANKL also led to the activation of Akt and eNOS and to NO production in endothelial cells (ECs). These effects were suppressed by the inhibition of TRAF6, phosphoinositide 3′-kinase (PI3K), Akt, or NOS by genetic or pharmacologic means. Inhibition of the TRAF6-mediated NO pathway reduced EC migration and capillary-like tube formation in response to RANKL. Moreover, the effects of RANKL on ECs sprouting from the aorta, and neovessel formation in both the mouse Matrigel plug assay and corneal micropocket assay, were impaired in eNOS-deficient mice. These results demonstrate that RANKL promotes vascular permeability and angiogenesis by stimulating eNOS by a TRAF6-PI3K-Akt–dependent mechanism. These properties may be relevant to the pathogenesis of angiogenesis-dependent and inflammatory vascular diseases. (Blood. 2007;109:000-000)

Introduction

Angiogenesis, the formation of new blood vessels from a preexisting vascular bed, is a pivotal process not only in embryonic development but also in the progression of a variety of pathologic conditions.[1] A large number of molecules, which are composed of growth factors, cytokines, and lipid metabolites, are shown to be involved in pathophysiologic neovascularization by stimulating endothelial cells (ECs) directly or indirectly.[2] Some of these factors, including VEGF, often possess their abilities to increase vascular permeability and thus contribute to deteriorating tissue damage.

Receptor activator of nuclear factor (NF)–κB ligand (RANKL), also known as ODF, TRANCE, and OPGL, has well-understood roles in the skeletal and immune systems in which it induces osteoclast differentiation from hematopoietic precursors and regulates the function and survival of dendritic cells.[3] Recently, interest has grown in its physiologic and pathologic relevance to vascular biology.[4] Mounting evidence suggests that RANKL and its decoy receptor, osteoprotegrin (OPG), participate in multiple aspects of vascular calcification; for example, mice lacking OPG suffer late medial calcification of the renal and aortic arteries in addition to early onset osteoporosis.[5-7] Moreover, a role for the OPG/RANKL/RANK axis in atherogenesis and plaque destabilization has been recently reported.[8] OPG inactivation accelerates advanced atherosclerotic lesion progression and calcification in older ApoE$^{-/-}$ mice.[9] TRANCE is strongly expressed in vascular cells in vitro, as well as in vivo. OPG and it are induced by inflammatory cytokines in human endothelial cells (ECs), although with different temporal profiles.[10] In vivo, RANKL is present in the small blood vessels of the skin and in arterial smooth muscle cells,[11] and it appears to be up-regulated in atherosclerotic lesions, calcified vessels, and valves.[4,6,9] Moreover, the RANKL receptor, RANK, is also expressed in ECs of the rat coronary artery and developing blood vessels of the rat embryo in vivo, as well as in freshly isolated human umbilical vein ECs (HUVECs).[12] In agreement with these patterns of expression, RANKL stimulates the survival of cultured ECs and their production of inflammatory cell adhesion molecules; it also promotes in vitro angiogenesis by the ECs and elicits neoangiogenesis in animal models.[1,3] Moreover, VEGF increases RANK mRNA and protein in ECs, augmenting their angiogenic response to RANKL.[12] Therefore, the RANKL/RANK/OPG system is believed to be an important link between the vascular, skeletal, and immune systems.

Endothelium-derived nitric oxide (NO), originally identified as endothelium-derived relaxing factor, promotes angiogenesis and

Submitted June 14, 2006; accepted September 29, 2006. Prepublished online as *Blood* First Edition Paper, October 12, 2006; DOI 10.1182/blood-2006-06-029298.

The online version of this article contains a data supplement.

The publication costs of this article were defrayed in part by page charge payment. Therefore, and solely to indicate this fact, this article is hereby marked "advertisement" in accordance with 18 USC section 1734.

plays an important role in vascular remodeling and the maintenance of vascular integrity.[14,15] In ECs, NO is a product of the conversion of L-arginine to citrulline by endothelial NO synthase (eNOS). eNOS produces low levels of NO constitutively but can be transiently stimulated to produce high levels by various hormones and environmental stimuli such as vascular endothelial growth factor (VEGF), angiopoietin-1 (Ang-1), shear stress, and hypoxia.[16,17] Moreover, eNOS knockout (KO) mice exhibit impaired postnatal angiogenesis in response to tissue ischemia.[15,16] Although the mechanisms by which it promotes angiogenesis is not fully elucidated, NO has emerged as an important modulator of endothelial activation underlying physiologic and pathologic angiogenesis and inflammation.

The increased expression of RANKL in the injured blood vessels suggests the involvement of RANKL in vascular pathophysiology. However, little information is available for its vascular function and underlying signaling mechanisms in ECs. In the present study, our data demonstrate that RANKL has a significant effect on vascular permeability, which is governed by interendothelial junctions between adjacent cells. We further present genetic and pharmacologic evidence that endothelium-derived NO plays a critical role in promoting the vascular permeability and angiogenesis induced by RANKL.

Materials and methods

Cell culture and reagents

HUVECs were isolated from human umbilical cord veins by collagenase treatment, as described previously,[18] and were used in passages 2 to 7. They were grown in M199 medium (Invitrogen, Carlsbad, CA) supplemented with 20% fetal bovine serum (FBS). Soluble RANKL (hCD8-conjugated form) was purified from insect cells as described previously.[15]

Endothelial-cell migration assay

Chemotactic motility of HUVECs was assayed as described previously.[19] Briefly, the lower surface of the filter was coated with 10 μg gelatin. Fresh M199 medium (1% FBS) containing RANKL was placed in the lower wells. The cells were trypsinized and suspended at a final concentration of 1×10^6 cells/mL in M199 containing 1% FBS. One hundred microliters of the cell suspension was loaded into each of the upper wells, and the chamber was incubated at 37°C for 4 hours. The cells were fixed and stained with hematoxylin and eosin. Nonmigrating cells on the upper surface of the filter were removed by wiping with a cotton swab, and chemotaxis was quantified with an optical microscope (× 200) by counting cells that had migrated to the lower side of the filter. Ten fields were counted for each assay.

Tube formation assay

Tube formation was assayed as previously described.[19] Briefly, 250 μL growth factor-reduced Matrigel (10 mg protein/mL) was pipetted into a 16-mm diameter tissue culture well and polymerized for 30 minutes at 37°C. HUVECs incubated in M199 containing 1% FBS for 6 hours were harvested after trypsin treatment, resuspended in M199, plated onto the layer of Matrigel at a density of 1.8×10^5 cells/well, and RANKL was added. After 20 hours, the cultures were photographed (× 200). The area covered by the tube network was measured using an optical imaging technique in which pictures of the tubes were scanned in Adobe Photoshop (San Diego, CA) and quantified with Image-Pro Plus (Media Cybernetics, Silver Spring, MD).

Retroviral vectors and generation of stable transfectants

cDNA sequences encoding hemagglutinin (HA)–tagged dominant-negative TRAF2 (DN-T2) and Flag-tagged dominant-negative TRAF6 (DN-T6) were subcloned into pMSCVpuro vector (Clontech, Palo Alto, CA) and introduced into HEK293T cells (packaging cell line) with 1 μg pVSV-G vector (Clontech) using LipofectAMINE Plus reagent according to the manufacturer's instructions. The next day, the virus in the supernatants of these cells was added to HUVECs along with 5 μg/mL polybrene. After 24 hours of incubation, the medium was removed and replaced with fresh medium containing 3 μg/mL puromycin. Puromycin-resistant clones were selected by incubating for 1 week in the presence of 3 μg/mL puromycin. Protein expression was confirmed by Western blotting.

[^{3}H] Sucrose permeability assay

HUVECs were plated onto a Transwell filter (Corning Costar, Acton, MA). After reaching confluence, HUVECs were incubated with M199 containing 1% FBS for 3 hours and treated with various concentrations of RANKL (0.5, 1, and 5 μg/mL) or 20 ng/mL VEGF for 1 hour. Fifty microliters (0.8 μCi [0.0296 MBq]/mL) of [^{3}H]sucrose (1 μCi [0.037 MBq]/μL; Amersham Pharmacia, Piscataway, NJ) was added to the upper compartment. The amount of radioactivity that diffused into the lower compartment was determined after 30 minutes by liquid scintillation counter (Wallac, Gaithersburg, MD; PerkinElmer, Wellesley, MA).

Miles vascular permeability assay

Miles assay was performed as described previously.[20] Evans blue dye (100 μL of a 1% solution in 0.9% NaCl) was injected into the tail vein of C57BL/6 wild-type (WT) and eNOS knockout (KO) mice (n = 7 per group). After 10 minutes, RANKL (10 μg in 10 μL PBS) was injected intradermally into the shaved back skin of mice. After 20 minutes, the animals were killed, and an area of skin that included the blue spot resulting from leakage of the dye was removed. Evans blue dye was extracted from the skin by incubation with formamide for 4 days at room temperature, and the absorbance of the extracted dye was measured at 620 nm with a spectrophotometer.

Perfusion of FITC-dextran

C57BL/6 WT and eNOS KO mice (8-10 weeks old, n = 7 per group) were examined for vascular leakage after injection of RANKL. RANKL (10 μg) or PBS was injected slowly into the vitreous cavity. After 24 hours, the mice were deeply anaesthetized using ketamine/xylazine and received an intravenous injection of 10 mg FITC-dextran (MW = 20 000 D; Sigma, St Louis, MO). After 30 minutes, the eyes were enucleated and immediately fixed in 4% paraformaldehyde. The retinas were dissected out, cut in a Maltese cross configuration, flat-mounted on glass slides, and viewed with a fluorescence microscope (Zeiss, Jena, Germany). The vascular permeability was quantified by counting sites with extravasation of fluorescence at postcapillary vessel.

VE-cadherin translocation assay

HUVECs plated in 6-well plates were serum starved in medium 199 containing 1% FBS for 6 hours. They were then stimulated with 5 μg/mL RANKL for 1 hour and fractionated in cytoskeleton-stabilizing buffer (10 mM HEPES [pH 7.4], 250 mM sucrose, 150 mM KCl, 1 mM EGTA, 3 mM $MgCl_2$, 1 × protease inhibitor cocktail [Roche Diagnostics, Indianapolis, IN], 1 mM Na_3VO_4, 0.5% Triton X-100) by centrifugation at 15 000*g* for 15 minutes. The proteins in the Triton X-100–insoluble and insoluble fractions were analyzed by Western blotting.

Measurement of nitrite plus nitrate

Production of nitrite plus nitrate (NOx) was measured by the ozone-chemiluminescence method. Culture media from HUVECs were collected and assayed for NOx using a chemiluminescent NO analyzer

(Antek Instruments, Houston, TX),[21] and quantified with sodium nitrate as standard.

eNOS activity assay

HUVECs were detached with PBS/EDTA (1 mM) and homogenized in 10 mM Tris-HCl pH 7.4. [^{3}H]-L-arginine to [^{3}H]-L-citrulline conversion was measured with 1 mM $CaCl_2$ with or without L-NAME (1 mM) using a NOS assay kit (Calbiochem, La Jolla, CA).

In vivo Matrigel plug assay

Matrigel plug assays were performed as previously described.[22] Briefly, WT and eNOS KO mice (n = 7 per group) were injected subcutaneously with 0.6 mL Matrigel containing RANKL and 15 U heparin. The injected Matrigel rapidly formed a single, solid gel plug. After 7 days, the skin of the mouse could be easily pulled back to expose the Matrigel plug, which remained intact. Hemoglobin was measured by the Drabkin method with Drabkin reagent kit 525 (Sigma) to quantify blood vessel formation. The concentration of hemoglobin was calculated from a known amount of hemoglobin assayed in parallel. To identify infiltrating endothelial cells, immunohistochemistry was performed with anti-CD31 antibody.

Aortic ring assay

Aortas were harvested from 6-week-old male Sprague Dawley rats, 6- to 8-week-old C57BL/6 wild-type (WT), and eNOS knockout (KO) mice. Plates (48-well) were coated with 100 μL Matrigel, and, after it had gelled, the rings were placed in the wells and sealed in place with an overlay of 40 μL Matrigel. RANKL and inhibitors were added to the wells in a final volume of 200 μL human endothelial serum-free medium (Invitrogen). On day 6, cells were fixed and stained with Diff-Quick. The assays were scored, double blind, from 0 (least positive) to 5 (most positive). Each data point was assayed in sextuplet.

Mouse corneal angiogenesis assay

Eight-week-old male C57BL/6 WT and eNOS KO mice (n = 7 per group) were used. After systemic and local eye anesthesia, a central, intrastromal linear keratotomy approximately 0.6 mm in length was performed with a surgical blade, and a micropocket was dissected toward the temporal limbus with a modified von Graefe knife. A sucrose aluminum sulfate pellet coated with Hydron polymer containing control buffer or RANKL (10 μg/pellet) was positioned 0.6 to 0.8 mm from the corneal limbus. On postoperative day 6, we measured the arc of the corneal circumference occupied by angiogenesis (circumferential angiogenesis, in degrees) and vessel lengths and numbers.

Leukocyte infiltration

Eight-week-old male C57BL/6 WT and eNOS KO mice were anesthetized and received a topical application of RANKL (3 μg/mL) or PBS. Twenty-four hours after RANKL application, the retroorbital venous sinus of each animal was injected intravenously with 200 μL biotinylated *Lycopersicon esculentum* lectin (1 mg/mL; Vector Laboratories, Burlingame, CA), which binds to *N*-acetyl-D-glucosamine residues on the luminal surface of vascular endothelial cells.[23] To perfuse the mice, the chest cavity was opened, and the atria were cut to allow outflow of blood and perfusate. Mice were perfused with a fixative (1% paraformaldehyde, 0.5% glutaraldehyde in PBS) via the left ventricle. The ears were removed, and the vascular architecture was analyzed in whole mounts of mouse ears, using a ZEISS AxioSkop2 microscope. Images of blood vessels and infiltrated leukocytes were captured, using a ZEISS AxioCam.

Statistical analysis

Data are presented as mean ± SD or ± SE. Statistical comparisons between groups were performed using one-way ANOVA followed by Student *t* test.

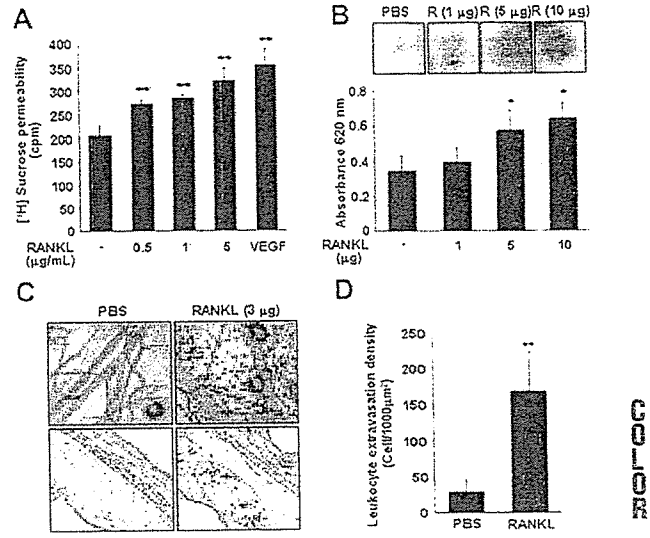

Figure 1. RANKL induces vascular hyperpermeability and leukocyte extravasation. (A) An in vitro [^{3}H]sucrose permeability assay was performed as described in "Materials and methods." Three independent experiments were performed in duplicate. Data are means − SEs; $^{**}P < .01$ versus untreated control. (B) In vivo Miles vascular permeability assay. Various concentrations of RANKL (R) or PBS were injected intradermally into the skin of C57BL/6 mice (n = 7 per group) after intravenous injection of Evans blue. Representative picture (top) and quantity (bottom) of extravasated Evans blue in the mouse skin. Data are means ± SDs; $^{*}P < .05$ versus PBS. (C) Leukocyte extravasation. Twenty-four hours after RANKL (3 μg) application as described in "Materials and methods," mice (n = 5 per group) were perfused with the lectin *L esculentum* to visualize extravasated leukocytes (top). This experiment was performed twice. Leukocytes in the ear sections were immunostained with anti-CD11a antibody (bottom). Arrows indicate extravasated CD11a$^+$ leukocytes. (D) Quantitative analysis of extravasated leukocytes. Data are means ± SDs; $^{**}P < .01$ versus PBS.

Results

RANKL induces vascular hyperpermeability and leukocyte extravasation

Human CD8-conjugated soluble RANKL increased [^{3}H] sucrose diffusion through the pores of Transwell membranes in HUVEC monolayer culture in a dose-dependent manner (Figure 1A). The near maximal activity at 5 μg/mL was comparable to that achieved with 20 ng/mL VEGF. To test whether RANKL induces vascular hyperpermeability in vivo, a modified Miles vascular permeability assay was performed using intravenous injection of Evans blue followed by intradermal injection of RANKL. RANKL strongly induced vascular hyperpermeability in the mouse skin, as shown by the increased leakage of Evans blue (Figure 1B). Spectrophotometric measurements of the extravasated Evans blue revealed that the increase was dose dependent (Figure 1B). We further investigated the effect of RANKL on leukocyte extravasation in vivo. The mice received an ear inoculation of vehicle or RANKL for 24 hours, and then leukocyte infiltration was monitored by in vivo perfusions with the lectin *L esculentum*. RANKL-treated mice showed a dramatic increase in leukocyte extravasation, as compared with vehicle-treated mice (Figure 1C). The identity of extravasated leukocytes was confirmed by CD11a staining in the ear section (Figure 1D).

Impairment of RANKL-induced vascular hyperpermeability in eNOS-deficient mice

The role of endothelial NO in RANKL-induced vascular permeability was evaluated. The NO synthase inhibitor NMA

tapraid4/zh8-bloo/zh8-bloo/zh800407/zh80803d07g | sangreyj | S=4 | 12/9/06 | 19:57 | Art: 2006/029298 | Input-DCT-???

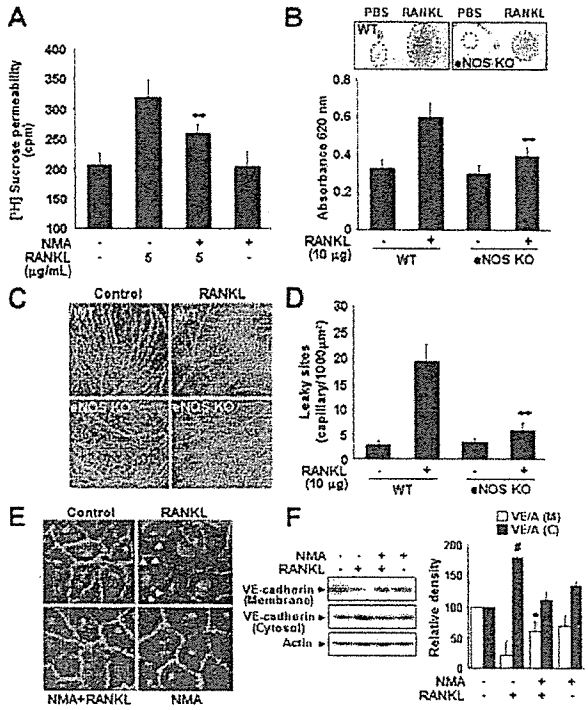

Figure 2. Impairment of RANKL-induced vascular hyperpermeability in eNOS-deficient mice. (A) HUVECs were preincubated for 30 minutes with or without NMA (1 mM) and stimulated with 5 μg/mL RANKL for 1 hour. A [³H]sucrose permeability assay was then performed. Three independent experiments were performed in duplicate. Data are means ± SEs: $^{**}P < .01$ versus RANKL alone. (B) An in vivo Miles vascular permeability assay was performed in WT and eNOS KO mice (n = 7 per group) as described in Figure 1. Data are means ± SDs; $^{**}P < .01$ versus RANKL in eNOS KO. (C) Representative fluorescence images of retinal vessels. RANKL (10 μg) or PBS was injected into the vitreous cavity of WT and eNOS KO mice (n = 7 per group). After 24 hours, the mice received an intravenous injection of 10 mg FITC-dextran (MW = 20 000 D), and their retinas were flat-mounted. (D) The vascular permeability was quantified by counting sites with extravasation of fluorescence at postcapillary vessel. Data are means ± SDs; $^{**}P < .01$ versus RANKL in eNOS KO. (E-F) HUVECs were preincubated for 30 minutes with or without NMA (1 mM) and stimulated with 5 μg/mL RANKL for 1 hour. (E) An immunofluorescence analysis of VE-cadherin. (F) Translocation of VE-cadherin was assessed as described in "Materials and methods." The Triton X-100–insoluble and soluble fractions were subjected to SDS–polyacrylamide gel electrophoresis (PAGE) followed by Western blot analysis with anti–VE-cadherin. Blots are representative of 3 independent experiments. Densitometric analyses are presented as the relative ratio of VE-cadherin to actin. VE indicates VE-cadherin; A, actin; M, membrane; C, cytosol. Data are means ± SDs: $^{*}P < .05$ versus RANKL alone; $^{\#}P < .05$ versus untreated control.

significantly abrogated RANKL-induced endothelial permeability in vitro (Figure 2A). Consistently, vascular hyperpermeability of the mouse skin by RANKL was substantially impaired in the eNOS KO mice compared with WT mice (Figure 2B). We further investigated the role of eNOS in retinal vascular permeability that is caused by breakdown of tight junctions between the retinal vascular endothelial cells. As shown in Figure 2C-D, injection of RANKL into the vitreous cavity of WT mice induced marked retinal vascular leakage as evidenced by the widespread, diffuse fluorescence. By contrast, the retinal vessels of the eNOS KO mice remained clearly delineated, with little or no leakage. Furthermore, the effect of RANKL on leukocyte extravasation in vivo was significantly abrogated in eNOS KO mice compared with WT mice (Figure S1A-B, available on the *Blood* website; see the Supplemental Figures link at the top of the online article).

Vascular endothelial permeability is maintained by the endothelial junction proteins, VE-cadherin, and occludin.[24] The effect of RANKL on adherens junction (AJ) formation was examined by immunostaining with anti–VE-cadherin. In confluent ECs, VE-cadherin is located at cell-cell contacts. When HUVECs were treated with RANKL, the level of VE-cadherin at cell-cell junctions markedly decreased, and pretreatment with NMA blocked this effect (Figure 2E). Normally, VE-cadherin that is anchored to the actin cytoskeleton is detected in the detergent-insoluble fractions of cell lysates.[25] There was a decrease in VE-cadherin in the Triton X-100–insoluble fraction and a concomitant increase in the Triton X-100–soluble fraction after stimulation with RANKL. This effect was reversed by NMA (Figure 2F). Taken together, these results demonstrate that RANKL induces vascular hyperpermeability in an NO-dependent manner by promoting the breakdown of endothelial AJs.

RANKL induces eNOS activation and NO production via a TRAF6/PI3K/Akt signaling pathway

To confirm whether RANKL stimulates NO production in endothelial cells, quiescent HUVECs were stimulated with RANKL and assayed for NO production and eNOS activity. RANKL increased NO production and eNOS activity (Figure 3A-B), without affecting the expression of eNOS protein (Figure 3C). The eNOS activity was evidently increased at 0.5 hours after RANKL treatment and sustained up to 24 hours (Figure 3B). eNOS is an isoform of NO

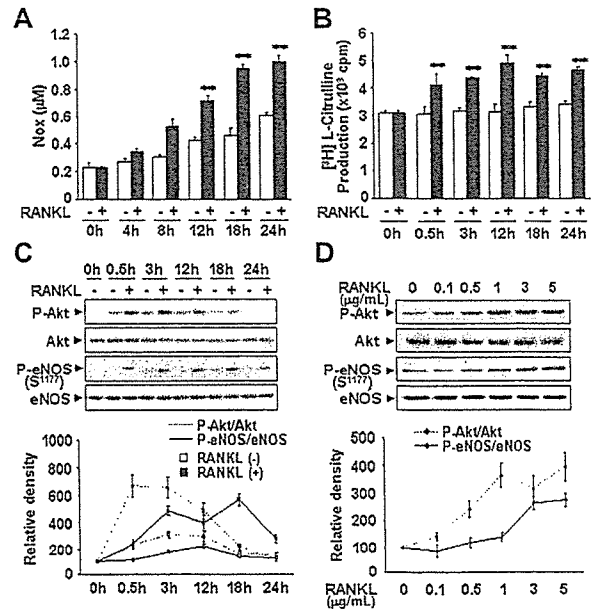

Figure 3. RANKL induces eNOS activation and NO production in endothelial cells. (A-D) HUVECs were stimulated with 5 μg/mL RANKL for the indicated times (A-C) and with various concentrations of RANKL for 30 minutes (D). (A) Levels of NOx was determined in the culture medium by using a chemiluminescent NO analyzer. (B) The eNOS enzymatic activity was measured by the production of [³H]-L-citrulline from [³H]-L-arginine. Three independent experiments were performed in duplicate. Data are means ± SEs. Statistical analysis of the results was carried out using ANOVA. $^{**}P < .01$ versus untreated control in 0 hour and each time point. (C-D) The levels of eNOS protein and phosphorylation of Akt and eNOS by RANKL were determined by Western blotting (top). Blots are representative of 3 independent experiments. Densitometric analyses are presented as the relative ratio of P-Akt to Akt and P-eNOS to eNOS. The relative ratio in untreated control is arbitrarily presented as 100 (bottom).

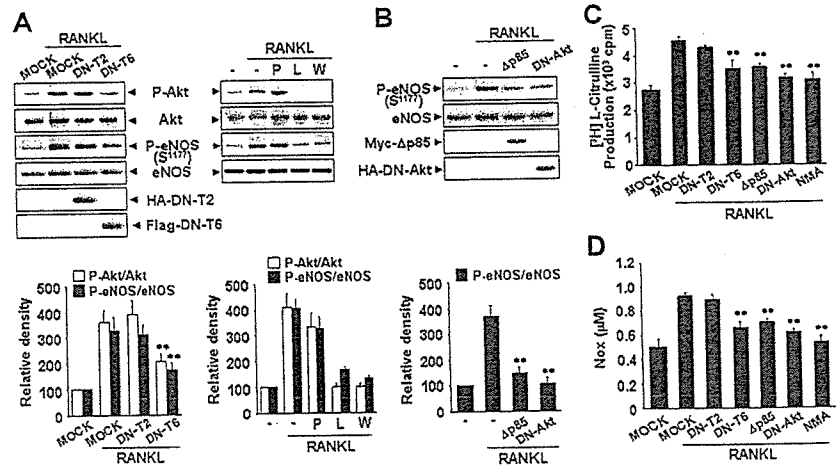

Figure 4. RANKL induces eNOS activation and NO production via a TRAF6/PI3K/Akt signaling pathway. (A) HUVECs were stably transfected with a HA-tagged DN-T2 and a Flag-tagged DN-T6 using retroviral system (left). HUVECs were preincubated for 30 minutes with or without 5 μM PP1, 100 nM Wortmannin, or 1 mM NMA prior to stimulation with RANKL (5 μg/mL) for 20 minutes (right). (B) HUVECs were transiently transfected with a HA-tagged DN-Akt or a Myc-tagged Δp85. (A-B) The levels of eNOS protein and the phosphorylation of Akt and eNOS by RANKL were determined by Western blotting (top). Blots are representative of 3 independent experiments. Densitometric analyses are presented as the relative ratio of P-Akt to Akt and P-eNOS to eNOS (bottom). (C-D) eNOS activity and NO production were measured as described in Figure 3A-B. Three independent experiments were performed in duplicate. Data are means − SDs: $^{**}P < .01$ versus RANKL alone.

synthase that is constitutively expressed in HUVECs and activated by Akt-mediated phosphorylation at Ser1177.[26,27] When HUVECs were exposed to RANKL, there was a dose-dependent increase in phosphorylation of eNOS at Ser1177 (Figure 3D). The increase was detected within 10 minutes, reached a maximum at 20 to 30 minutes, and was sustained for nearly 24 hours (Figure 3C). Consistent with this, we detected an increase in Akt phosphorylation (Figure 3C-D). However, other phosphorylation sites of eNOS were not changed by RANKL treatment (Figure S2).

We further analyzed the signaling mechanism involved in RANKL-induced eNOS phosphorylation and NO production. RANK, like other TNFR family members, lacks catalytic activity and interacts with TRAFs that act as adaptors activating downstream signaling pathways. Of the TRAFs, TRAF2 and TRAF6 appear to be important components of the RANKL signaling pathway.[28] Overexpression of DN-T6 resulted in substantial inhibition of eNOS phosphorylation, eNOS activity, and NO production, whereas DN-T2 had no effect (Figure 4A,C-D). Recruitment of TRAF6 to the cytoplasmic domains of RANK can lead to the activation of PI3K that subsequently links to Akt pathway. Indeed, the PI3K inhibitors, LY294002 and Wortmannin, markedly inhibited RANKL-induced eNOS phosphorylation, whereas PP1, a potent Src tyrosine kinase inhibitor, had no effect (Figure 4A). Consistently, overexpression of Δp85, a dominant-negative mutant of the p85 regulatory subunit of PI3K, and DN-Akt, a dominant-negative mutant of Akt, inhibited RANKL-induced eNOS activation (Figure 4B-D). Taken together, these results indicate that RANKL stimulates the production of endothelial NO via a TRAF6-dependent PI3K/Akt signaling pathway acting on eNOS.

NO is required for RANKL-induced migration and capillary-like network by ECs

RANKL induced the formation of extensive capillary-like networks of ECs cultured on 2-D Matrigel matrix, and this effect was almost completely inhibited by pretreatment with NMA (Figure 5A-B). Consistent with involvement of the eNOS activation pathway, RANKL-induced capillary-like network was blocked by Wortmannin, as well as by overexpression of DN-T6, but not of DN-T2 (Figure 5C-D). We next examined the role of NO in RANKL-induced EC migration. RANKL stimulated the chemotactic motility of HUVECs approximately 1.5-fold, and this effect was

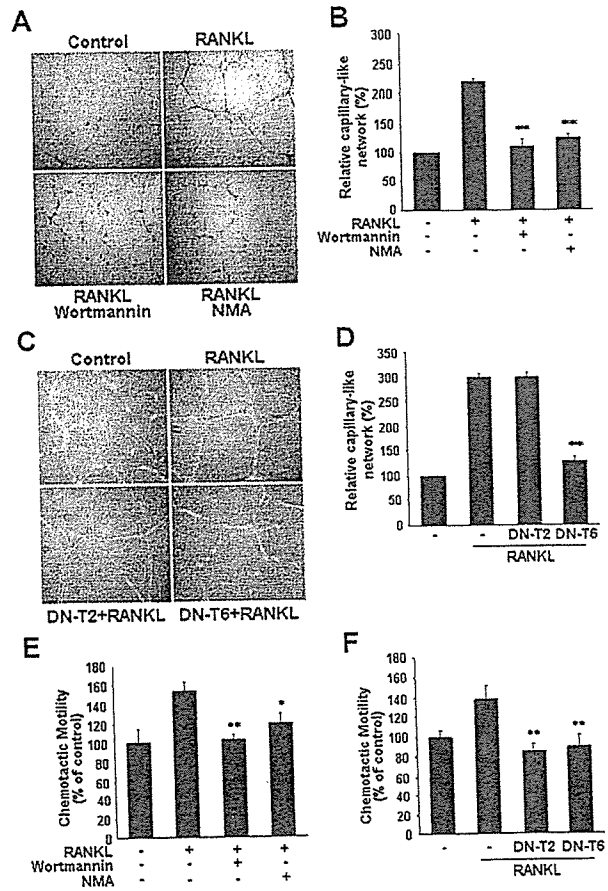

Figure 5. Involvement of PI3K/Akt-dependent NO production in RANKL-induced migration and capillary-like network by ECs. (A,E) HUVECs were preincubated for 30 minutes with or without 100 nM Wortmannin or 1 mM NMA prior to stimulation with RANKL (5 μg/mL). (C, F) HUVECs were stably transfected with DN-T2 and DN-T6 using retroviral system. (A,C) Cells were plated on Matrigel-coated plates at a density of 2×10^5 cells/well and incubated with 5 μg/mL RANKL. Microphotographs were taken after 20 hours (× 200). (B,D) Capillary-like networks were quantified with Image-Pro Plus software. (E-F) After 4 hours of incubation, chemotaxis was quantified with an optical microscopy. Three independent experiments were performed in duplicate. Data are means − SDs: $^{*}P < .05$; $^{**}P < .01$ versus RANKL alone.

tapraid4/zh8-bloo/zh8-bloo/zh800407/zh80803d07g | sangreyj | S=4 | 12/9/06 | 19:57 | Art: 2006/029298 | Input-DCT-???

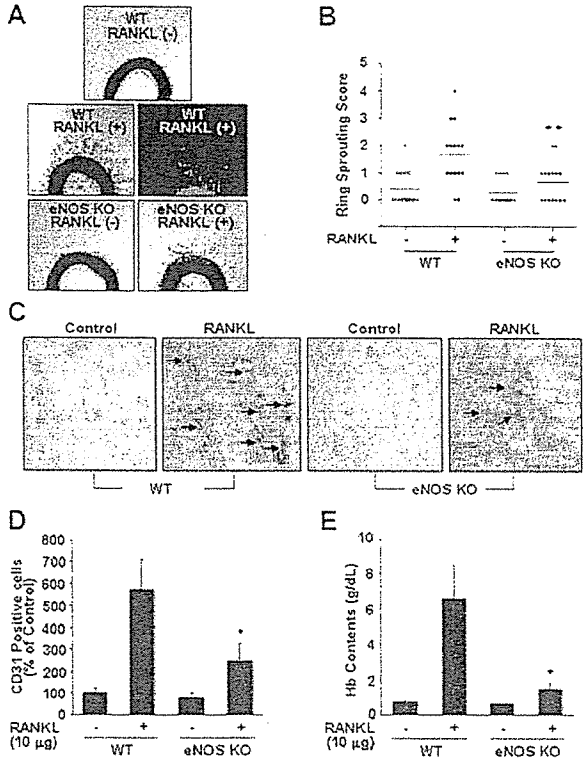

Figure 6. eNOS plays a critical role in RANKL-induced angiogenesis. (A) Aortic segments were harvested from WT and eNOS KO mice (n – 7 per group). Endothelial-cell sprouts forming branching cords from the margins of vessel segments taken from mice were photographed under a phase microscope. Staining of endothelial cells sprouted from RANKL-treated aorta with VWF (middle). (B) Sprouting scores were classified from 0 (least positive) to 5 (most positive). Data are means · SEs. (C-E) WT and eNOS KO mice (n – 7 per group) were injected with 0.6 mL Matrigel containing RANKL (10 μg). After 7 days, the mice were killed and the Matrigel plugs were excised. (C) Plugs were stained for infiltrating endothelial cells using anti-CD31 antibody. Arrows indicate CD31 · cells. (D) Quantitative assessment of CD31 · endothelial cells. (E) Quantification of neovessel formation by measuring hemoglobin in the Matrigel. Data are means SDs; *P < .05; **P < .01 versus RANKL in WT.

abolished by Wortmannin and NMA, as well as by DN-T6 (Figure 5E-F). These results suggest that NO is required for the migration and differentiation of ECs in response to RANKL. In contrast to its lack of effect on EC capillary-like network, DN-T2 did inhibit the RANKL-induced increase in chemotactic motility of the HUVECs (Figure 5F), pointing to the involvement of NO-independent pathways activated by TRAF2 in RANKL-induced EC migration.

eNOS plays a critical role in RANKL-induced angiogenesis

To further assess the role of NO in RANKL-induced angiogenesis, we compared endothelial-cell sprouting in the aortic ring segments from eNOS KO and WT mice. RANKL caused a 3-fold increase in endothelial-cell sprouting in WT mice, but this effect was significantly abrogated in the aortic rings from eNOS KO mice (Figure 6A-B). Furthermore, RANKL-induced sprouting of endothelial cells in the rat aortic rings was stimulated by RANKL, and this angiogenic response was inhibited by simultaneous treatment with Wortmannin or NMA (Figure S3A-B). We further analyzed the role of endothelial cell–derived NO in RANKL-induced neovascularization in vivo. Matrigel containing RANKL was subcutaneously injected into WT and eNOS KO mice, and 7 days later the Matrigel plugs formed in the mice were excised and analyzed. There was nearly 70 g/L (7 g/dL) hemoglobin in the plugs of the WT mice, whereas those of the KO mice contained only about 18 g/L (1.8 g/dL) (Figure 6E). Plugs of the WT mice exhibited significantly higher densities of CD31 · endothelial cells than those of KO mice (Figure 6C-D). Consistently, in a corneal micropocket assay, RANKL was less angiogenic in the eNOS KO mice than in the WT mice as measured by the numbers of neovessels (Figure S4A-B).

Discussion

The present results have revealed a novel action of RANKL, namely that of increasing vascular permeability in vitro and in vivo. Moreover RANKL can be added to the list of NO-dependent endothelial stimuli that promote both vascular leakage and angiogenesis. Our findings have implications for the role of RANKL in vascular physiology. Given its considerable adverse effects in adults, such as arterial calcification and inflammatory activation enhancing leukocyte adhesiveness,[5,29] our findings underline the possibility that RANKL is implicated in the development of vascular diseases.

Atherosclerosis has many characteristics in common with inflammatory disease characterized by infiltration of activated immune cells into the intima.[30] We have recently demonstrated that RANKL causes adhesion of leukocytes to ECs as a consequence of increased expression of cell adhesion molecules such as ICAM-1 and VCAM-1 in the ECs.[29] RANKL is produced by various cells, including vascular cells and activated immune cells close to blood vessels, and it exists in either a cell-bound or a secreted form.[3] Its expression, together with OPG, is also modulated by various factors such as the inflammatory cytokines, TNF-α and IL-1β.[3] Under some circumstances, the ratio of RANKL to OPG in the vascular area increases, and this change may activate endothelial cells, which are thought to be involved in promoting the early stage of atherosclerotic inflammation, which is characterized by increased endothelial permeability, up-regulation of adhesion molecules, and transendothelial migration of leukocytes.[31,32] Moreover, considering that angiogenesis and calcification are common features of advanced atherosclerotic lesions, the angiogenic and calcifying activities of RANKL may contribute to the development of atheromatous vessels.[33] Notably, this notion was supported by recent studies showing the enhanced expression of RANKL both in clinical and experimental atherosclerosis.[8] mRNA levels of RANKL were increased in T cells in patients with unstable angina accompanied by increased expression of RANK in monocytes.[8] In the apoE$^{-/-}$ mice, RANKL is significantly expressed within the atherosclerotic plaques, whereas no RANKL immunostaining was detected in the nonatherosclerotic vessel wall.[8] Furthermore, Bennett et al[9] have demonstrated that OPG inactivation results in larger and more calcified advanced lesions in the innominate arteries of older apoE$^{-/-}$ mice.

Vascular permeability is defined as the movement of fluids and molecules between blood vessels and the underlying tissues, and it is regulated by various inflammatory factors that break down intercellular endothelial junctions.[34] Although vascular leakage is not a prerequisite for blood vessel growth, increased vascular permeability often coincides with the early stage of angiogenesis and is also found in areas of diseased tissue in diabetic retinopathy, solid tumors, myocardial infarction, wounds, and chronic inflammation.[35] VEGF, originally isolated as a vascular permeability factor

tapraid4/zh8-bloo/zh8-bloo/zh800407/zh80803d07g | sangreyj | S=4 | 12/9/06 | 19:59 | Art: 2006/029298 | Input-DCT-???

(VPF), is the best known angiogenic stimulus increasing the vascular permeability of microvessels to circulating macromolecules.[16] This VPF activity is correlated with various vascular pathophysiologies.[34] In contrast, endothelial permeability is not directly affected by bFGF and PDGF, or inhibited by angiopoietin-1, despite their prominent angiogenic activities.[35,36] Our data show that the effect of RANKL on endothelial permeability is comparable to that of VEGF. Because RANKL does not increase VEGF expression in ECs,[13] RANKL-induced endothelial permeabilization and angiogenesis appear to be exerted by a direct action on ECs, independent of VEGF. Note that injection of RANKL, like VEGF, into the vitreous cavity causes breakdown of the blood-retinal barrier formed by tight junctions between the retinal vascular endothelial cells, even though the mode of action of RANKL on the retinal vasculature is unknown.

It is interesting that the effects of RANKL on ECs are so similar to those of VEGF. VEGF was originally isolated from the vasculature and was shown to play essential roles in vascular physiology during embryonic development, as well as in the evolution of various diseases of adult vasculature. It has been found that VEGF is also capable of directly enhancing osteoclastic bone resorption and promoting the survival of mature osteoclasts.[37] Conversely, although RANKL was discovered as a factor active in bone remodeling, its role in vascular disease is increasingly recognized.[38] For example, inhibition of RANKL with OPG or RANK fusion proteins or RANKL antibodies reduced chronic inflammatory disorders and malignant tumors in animal models, in addition to bone loss caused by osteoporosis.[38] Our current and previous findings that RANKL promotes vascular permeabilization, angiogenesis,[13] and proinflammatory activation provide further evidence of the adverse effects of RANKL on adult vasculature.[29]

Our data also demonstrate the prominent roles of eNOS in RANKL-induced angiogensis and vascular permeability in vitro and in vivo. Many angiogenic factors, but not all, use NO as mediator in their angiogenic effects. Treatment of ECs with RANKL increased NO production, together with increased eNOS activity (Figure 3A-B). Blockage of NO release prevented RANKL-induced EC migration and capillary-like network formation in vitro, as well as sprouting of ECs from rat aorta (Figure 5; Figure S3). Both the mouse Matrigel plug assay and the cornea micropocket assay revealed that RANKL-induced neovascularization was substantially impaired in eNOS KO animals (Figure 6; Figure S4). Thus, it is clear that NO generated from eNOS is required for angiogenic responses to RANKL. The signaling mechanism involved in vascular permeabilization is complex and involves a wide array of factors that affect cell-cell junctions, cell-matrix interaction, and cytoskeletal organization. Involvement of protein kinase C (PKC) and Rho-mediated signaling pathways has been demonstrated in the endothelial permeability induced by various stimuli.[39] NO also seems important in mediating vascular permeability, but this is context dependent. In ischemia-reperfusion injury models, NO has been shown to maintain vessel integrity.[15] However, it increased vascular permeability in tumors and in chronic inflammation.[35] Our present data indicate that NO plays an important role in RANKL-induced vascular permeability because vascular leakage in the skin of mice and in the retina induced by RANKL was significantly reduced in eNOS KO mice, and these in vivo findings were confirmed by measuring permeability and VE-cadherin junction in cultured endothelial cells. However, RANKL-induced permeability was not completely blocked by inhibiting NO production, pointing to the contribution of other signaling components such as PKC, which is activated in ECs by RANKL.[29]

RANKL causes NO production by ECs via PI3K/Akt-dependent eNOS activation (Figure 4A-D). Although eNOS is constitutively expressed in ECs, its activity can be modulated by variation in its level of expression or by reversible phosphorylation on Ser1177.[27] Treatment of ECs with RANKL did not alter the levels of eNOS mRNA and protein (Figure 3C). However, it led to phosphorylation of eNOS at Ser1177, a major phosphorylation site for Akt, and this was blocked by a dominant-negative form of Akt. Moreover, blockage of either PI3K or Akt resulted in a significant reduction in NO production in response to RANKL. Recently, we demonstrated the involvement of Src and PLC pathway in RANKL-induced angiogenesis.[13] However, the Src inhibitor PP1 had no effect on RANKL-induced eNOS activation, indicating that Src is not upstream of the Akt/eNOS pathway by RANKL. Our data also point to a predominant role of TRAF6 in the RANKL-induced NO production. Previous studies in nonendothelial cells have shown that TRAF adaptor proteins such as TRAF2, TRAF5, and TRAF6 can associate with the cytoplasmic tail of RANK and activate various intracellular signaling pathways.[28] We have recently demonstrated that TRAF2 and TRAF6 play an important role in RANKL-induced NF-κB activation in endothelial cells, which leads to increased endothelial CAM expression and EC-leukocyte interactions.[29] Surprisingly, a dominant-negative form of TRAF6 but not of TRAF2 inhibited NO production and phosphorylation of Akt and eNOS. Because PI3K mediates Akt phosphorylation, TRAF6 probably links the membrane receptor RANK to PI3K in ECs. Therefore, these results suggest a multifaceted role of TRAF6 in the RANK-mediated angiogenic and inflammatory signaling pathways in ECs.

In summary, the present study provides the first evidence that RANKL increases endothelial permeability in addition to stimulating angiogenesis as previously shown, and it reveals that these effects are dependent on endothelium-derived NO. These findings suggest that elevated RANKL levels in the vascular area may lead directly to endothelial activation and may make an important contribution to the occurrence of angiogenesis-dependent inflammatory vascular diseases such as atherosclerosis.

Acknowledgments

This work was supported by Korea Biotech R&D Group of MoST (Ministry of Science and Technology) (research grant M10416130002-04N1613-00210), the Korea Research Foundation of Korean Government (Ministry of Education and Human Resources Development [MOEHRD]) (grant KRF-2003-C00054), Molecular Cellular Biodiscovery Research Group of MoST (grant 2004-01587), and Vascular System Research Center grant from KOSEF.

Authorship

Contribution: J.-K.M. and Y.-G.K. designed the research; J.-K.M., Y.-L.C., J.-H.C., Y.K., and J.H.K. performed the research; Y.-G.K. and J.R. contributed material; J.-K.M., Y.-G.K., and Y.S.Y. collected data; J.-K.M., Y.-G.K., N.M., Y.-M.K., and G.T.O. analyzed data; and J.-K.M. and Y.-G.K. wrote the paper.

Conflict-of-interest disclosure: The authors declare no competing financial interests.

Correspondence: Young-Guen Kwon, Department of Biochemistry, College of Sciences, Yonsei University, Seoul, 120-749, Republic of Korea; e-mail: ygkwon@yonsei.ac.kr.

References

1. Folkman J. Angiogenesis in cancer, vascular, rheumatoid and other disease. Nat Med. 1995;1: 27-31.
2. Moulton KS, Heller E, Konerding MA, Flynn E, Palinski W, Folkman J. Angiogenesis inhibitors endostatin or TNP-470 reduce intimal neovascularization and plaque growth in apolipoprotein E-deficient mice. Circulation. 1999;99:1726-1732.
3. Walsh MC, Choi Y. Biology of the TRANCE axis. Cytokine Growth Factor Rev. 2003;14:251-263.
4. Sattler AM, Schoppet M, Schaefer JR, Hofbauer LC. Novel aspects on RANK ligand and osteoprotegerin in osteoporosis and vascular disease. Calcif Tissue Int. 2004;74:103-106.
5. Bucay N, Sarosi I, Dunstan C, et al. Osteoprotegerin-deficient mice develop early onset osteoporosis and arterial calcification. Genes Develop. 1998;12:1260-1268.
6. Min H, Morony S, Sarosi I, et al. Osteoprotegerin reverses osteoporosis by inhibiting endosteal osteoclasts and prevents vascular calcification by blocking a process resembling osteoclastogenesis. J Exp Med. 2000;192:463-474.
7. Collin-Osdoby P. Regulation of vascular calcification by osteoclast regulatory factors RANKL and osteoprotegerin. Circ Res. 2004;95:1046-1057.
8. Sandberg WJ, Yndestad A, Oie E, et al. Enhanced T-cell expression of RANK ligand in acute coronary syndrome: possible role in plaque destabilization. Arterioscler Thromb Vasc Biol. 2006; 26:857-863.
9. Bennett BJ, Scatena M, Kirk EA, et al. Osteoprotegerin inactivation accelerates advanced atherosclerotic lesion progression and calcification in older ApoE-/- mice. Arterioscler Thromb Vasc Biol. 2006;26:2117-2124.
10. Collin-Osdoby P, Rothe L, Anderson F, Nelson M, Maloney W, Osdoby P. Receptor activator of NF-κB and osteoprotegerin expression by human microvascular endothelial cells, regulation by inflammatory cytokines, and role in human osteoclastogenesis. J Biol Chem. 2001;276:20659-20672.
11. Kartsogiannis V, Zhou H, Horwood NJ, et al. Localization of RANKL (receptor activator of NF-κB ligand) mRNA and protein in skeletal and extraskeletal tissues. Bone. 1999;25:525-534.
12. Min JK, Kim YM, Kim YM, et al. Vascular endothelial growth factor up-regulates expression of receptor activator of NF-kappaB (RANK) in endothelial cells. Concomitant increase of angiogenic responses to RANK ligand. J Biol Chem. 2003; 278:39548-39557.
13. Kim YM, Kim YM, Lee YM, et al. TNF-related activation-induced cytokine (TRANCE) induces angiogenesis through the activation of Src and phospholipase C (PLC) in human endothelial cells. J Biol Chem. 2002;277:6799-6805.
14. Rudic RD, Shesely EG, Maeda N, Smithies O, Segal SS, Sessa WC. Direct evidence for the importance of endothelium-derived nitric oxide in vascular remodeling. J Clin Invest. 1998;101:731-736.
15. Murohara T, Asahara T, Silver M, et al. Nitric oxide synthase modulates angiogenesis in response to tissue ischemia. J Clin Invest. 1998; 101:2567-2578.
16. Fukumura D, Gohongi T, Kadambi A, et al. Predominant role of endothelial nitric oxide synthase in vascular endothelial growth factor-induced angiogenesis and vascular permeability. Proc Natl Acad Sci U S A. 2001;98:2604-2609.
17. Jaffe EA, Nachman RL, Becker CG, Minick CR. Culture of human endothelial cells derived from umbilical veins. Identification by morphologic and immunologic criteria. J Clin Invest 1973;52:2745-2756.
18. Wong BR, Rho J, Arron J, et al. TRANCE is a novel ligand of the tumor necrosis factor receptor family that activates c-Jun N-terminal kinase in T cells. J Biol Chem. 1997;272:25190-25194.
19. Lee OH, Kim YM, Lee YM, et al. Sphingosine 1-phosphate induces angiogenesis: its angiogenic action and signaling mechanism in human umbilical vein endothelial cells. Biochem Biophys Res Commun. 1999;264:743-750.
20. Oura H, Bertoncini J, Velasco P, Brown LF, Carmeliet P, Detmar M. A critical role of placental growth factor in the induction of inflammation and edema formation. Blood. 2003;101:560-567.
21. Braman RS, Hendrix SA. Nanogram nitrite and nitrate determination in environmental and biological materials by vanadium (III) reduction with chemiluminescence detection. Anal Chem. 1989; 61:2715-2718.
22. Drabkin DS, Ausin JH. Spectrophotometric constants for common hemoglobin derivatives in human, dog, and rabbit blood. J Biol Chem. 1932; 98:719-725.
23. Min JK, Lee YM, Kim JH, et al. Hepatocyte growth factor suppresses vascular endothelial growth factor-induced expression of endothelial ICAM-1 and VCAM-1 by inhibiting the nuclear factor-kappaB pathway. Circ Res. 2005;96:300-307.
24. Bazzoni G, Dejana E. Endothelial cell-to-cell junctions: molecular organization and role in vascular homeostasis. Physiol Rev. 2004;84:869-901.
25. Lee MJ, Thangada S, Claffey KP, et al. Vascular endothelial cell adherens junction assembly and morphogenesis induced by sphingosine-1-phosphate. Cell. 1999;99:301-312.
26. Shiojima I, Walsh K. Role of Akt signaling in vascular homeostasis and angiogenesis. Circ Res. 2002;90:1243-1250.
27. Dimmeler S, Fleming I, Fisslthaler B, Hermann C, Busse R, Zeiher AM. Activation of nitric oxide synthase in endothelial cells by Akt-dependent phosphorylation. Nature. 1999;399:601-605.
28. Chung JY, Park YC, Ye H, Wu H. All TRAFs are not created equal: common and distinct molecular mechanisms of TRAF-mediated signal transduction. J Cell Sci. 2002;115:679-688.
29. Min JK, Kim YM, Kim SW, et al. TNF-related activation-induced cytokine (TRANCE) enhances leukocyte adhesiveness; induction of ICAM-1 and VCAM-1 via TRAF and PKC-dependent NF-κB activation in endothelial cells. J Immunol. 2005;175:531-540.
30. Glass CK, Witztum JL. Atherosclerosis, the road ahead. Cell. 2001;104:503-516.
31. Ross R. Atherosclerosis—an inflammatory disease. N Engl J Med. 1999;340:115-126.
32. Crotti T, Smith M, Hirsch R, et al. Receptor activator NF-κB ligand (RANKL) and osteoprotegerin (OPG) protein expression in periodontitis. J Periodont Res. 2003;38:380-387.
33. Collett GD, Canfield AE. Angiogenesis and pericytes in the initiation of ectopic calcification. Circ Res. 2005;96:930-938.
34. Weis SM, Cheresh DA. Pathophysiological consequences of VEGF-induced vascular permeability. Nature. 2005;437:497-504.
35. Fukumura D, Yuan F, Endo M, Jain RK. Role of nitric oxide in tumor microcirculation. Blood flow, vascular permeability, and leukocyte-endothelial interactions Am J Pathol. 1997;150:713-725.
36. Thurston G, Rudge JS, Ioffe E, et al. Angiopoietin-1 protects the adult vasculature against plasma leakage. Nat Med. 2000;6:460-463.
37. Nakagawa M, Kaneda T, Arakawa T, et al. Vascular endothelial growth factor (VEGF) directly enhances osteoclastic bone resorption and survival of mature osteoclasts. FEBS Lett. 2000;473:161-164.
38. Hofbauer LC, Schoppet M. Clinical implications of the osteoprotegerin/RANKL/RANK system for bone and vascular diseases. JAMA. 2004;292: 490-495.
39. Mehta D, Rahman A, Malik AB. Protein kinase C-alpha signals rho-guanine nucleotide dissociation inhibitor phosphorylation and rho activation and regulates the endothelial cell barrier function. J Biol Chem. 2001;276:22614-22620.

PPARと誘導型シクロオキシゲナーゼの関係

Relationship between PPAR and COX-2

井上裕康
Hiroyasu INOUE
奈良女子大学生活環境学部食物栄養学科

◎アラキドン酸から生成されるプロスタグランジン(PG)は代表的な生理活性脂質である．15-deoxy-$\Delta^{12,14}PGJ_2$はPPARの内因性リガンド候補として報告され，さまざまな生理作用が見出されている．この分子は種々の蛋白質のシステイン残基に共有結合することによりPPARγリガンドとは異なる作用機構が報告されているが，PPARγリガンド結合部分に共有結合し，合成リガンドとは異なった作用をもつ可能性も報告された．一方著者らは，PG産生の律速酵素・誘導型シクロオキシゲナーゼの発現を抑制する天然物質の探索から赤ワインに含まれるポリフェノール・レスベラトロールを見出し，この分子がPPARαおよびγのデュアルアゴニストになることを報告した．アピゲニン(パセリ)，フムロン(ビールホップ)についても同様な性質をもつ．これらの知見は，生活習慣病予防の視点から分子作用機構の解明が期待されるとともに，PPARがさまざまな生理活性脂質のセンサーとして働いている可能性を示している．

Key word：プロスタグランジン，PPAR，シクロオキシゲナーゼ，レスベラトロール

シクロオキシゲナーゼ(COX)はプロスタグランジン(PG)産生の律速酵素で，アラキドン酸を基質にしてPGH_2を生成する反応を触媒する．非ステロイド性抗炎症薬の作用はCOX活性の阻害によるPG産生抑制に由来する．COXには構成型発現を示すCOX-1と誘導型COX-2の2種類のアイソザイムが存在する．COX-2の発現は炎症性刺激で迅速に誘導され，かつグルココルチコイドによって抑制されることから，炎症反応への関与が想定されている．さらに，COX-2ノックアウトマウスの解析や最近の臨床，疫学調査を含む研究などから，COX-2が発癌，Alzheimer病，循環器系疾患にも関与し，さまざまな役割を担っていることがしだいに明らかになってきた[1]．

グルココルチコイドや活性型ビタミンDなどは生理活性をもつ脂溶性物質であり，これらをリガンドとする核内受容体群はその構造上の相同性によってファミリーを形成している．PPARはこの核内受容体ファミリーに属するリガンド依存性転写因子で，3種類のサブタイプα，β(δ)，γが知られており，それぞれ異なった生理作用に寄与している[2]．さらに，リガンド存在下でPPARγは不安定化するのに対しPPARαは逆に安定化するとの報告があり，共通のリガンドに対しても異なる働きをもつ可能性がある．PPARのリガンド結合部位については結晶構造が決定され，ほかの核内受容体に比べ，リガンド結合ポケットが大きいと報告された[3]．この特徴がさまざまな脂溶性の物質をリガンドとして結合するPPARの性質に関与しており，一般的なホルモンと受容体の関係とは異なっていると考えられる．PPARγの内因性リガンド候補としてPGD_2の代謝産物15-deoxy-$\Delta^{12,14}PGJ_2$(15d-PGJ_2)が報告された[4,5]．また，アラキドン酸をはじめとする脂肪酸やその代謝産物，非ステロイド性抗炎症薬などもPPARのリガンドとして働く可能性が指摘され，食生活とも密接にかかわる核内受容体であることがわかってきた．

図1にCOX経路および，リポキシゲナーゼ経路でPPARのリガンドとして働く可能性があるも

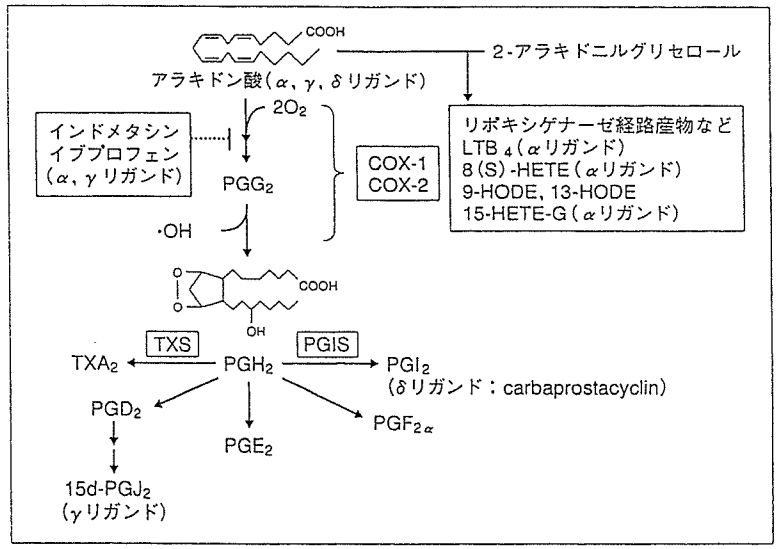

図 1　アラキドン酸カスケードとPPARリガンド

のを示す．注目すべきこととして，PPAR が関与していると考えられる生体内での役割は，前述した COX-2 が関与する役割と重複している点が多い．

マクロファージにおけるPPARγによるCOX-2発現のフィードバック制御

循環器系においては，プロスタサイクリン(PGI_2)とそれに拮抗する作用をもつトロンボキサン(TXA_2)の産生のバランスがホメオスタシスに重要であり，そのバランスの破綻は動脈硬化症をはじめとするさまざまな病態と関連している．PGI_2はおもに血管内皮細胞で，TXA_2は血小板や活性化マクロファージで産生されるが，血小板以外の細胞では COX-2 の発現が種々の刺激により誘導され，それぞれの PG 類産生に寄与している．著者らはその視点から，PGI_2を産生する培養血管内皮細胞と，TXA_2，PGE_2を産生するマクロファージ系 U937 細胞での COX-2 発現の相違に注目して研究を進めてきた[6,7]．

そのなかの研究で，U937 細胞において，COX-2 の発現がデキサメタゾン(DEX)や 15d-PGJ_2で抑制されること，その抑制効果は血管内皮細胞では認められないことを見出した[8,9]．U937 細胞におけるこの抑制効果は，それぞれの受容体であるグルココルチコイド受容体(GR)，PPARγ の発現に依存していたが，100 nM DEX では COX-2 の発現が 90％以上抑制されるのに対し，10 μM 15d-PGJ_2では 60％程度の抑制しか観察されない．GR mRNA の発現はリポポリサッカライド(LPS)刺激で上行制御されるのに対し PPARγ は逆に下行制御されること(図 2)から，DEX と 15d-PGJ_2の COX-2 発現抑制効果の相違は，核内受容体 GR と PPARγ の発現量が関与していること，さらに GR と PPARγ の 2 種類の核内受容体は COX-2 の発現に関して異なった役割をもつと考えられる．

つまり LPS 刺激により COX-2 が誘導され，多量の PG が産生された状態(活性化マクロファー

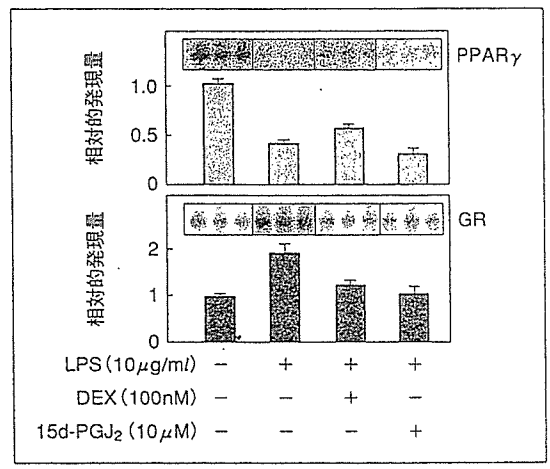

図 2　逆の発現パターンを示すPPARγとグルココルチコイド受容体mRNA[9]

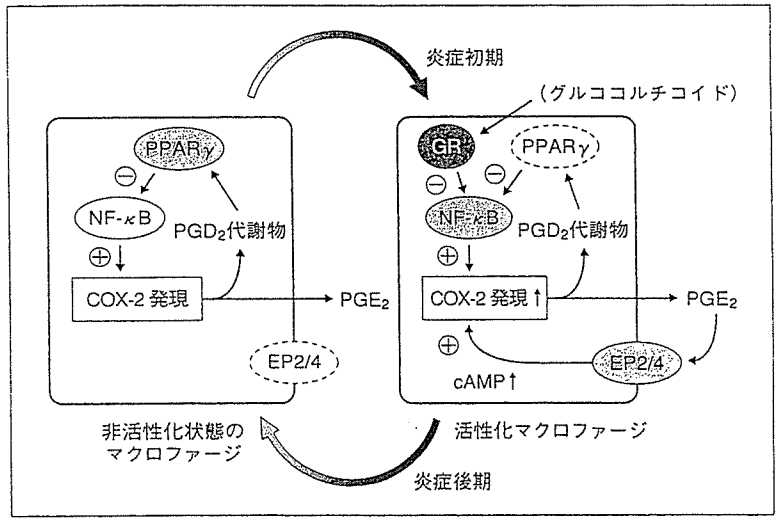

図 3　PPARγを介するCOX-2発現のフィードバック制御[9]

ジ)において，GR の発現上昇によって DEX に対する COX-2 の発現抑制感受性が上がる．それに対して，PPARγ は LPS 刺激で下行制御されるため 15d-PGJ_2に対する感受性は低下する．一方，活性化される前のマクロファージ(応答性マクロファージ)では 15d-PGJ_2が COX-2 の発現を抑制していると考えられる．さらに，このような細胞では造血器型 PGD 合成酵素が発現しており，15d-PGJ_2の前駆体となる PGD_2が COX-2 に依存して産生されることを見出した．これらの知見からマクロファージにおいては PGD_2代謝産物が PPARγ のリガンドとして作用することによって負のフィードバック制御を受けることが示唆された(図 3)．

一方，活性化状態になり PPARγ によるフィードバック制御から開放された COX-2 の発現は PGE_2の産生を促し，それがマクロファージ系細胞で発現する細胞膜型受容体 EP2 あるいは EP4 に働き，細胞内 cAMP 濃度を上昇させ，COX-2 の発現を増強する．このように，時間により異なる種類の PG 産生が核内受容体と細胞膜型受容体へ異なる情報を伝達することで，マクロファージにおけるダイナミックな PG 産生を可能にしていると考えられる[9,10]．

最近 COX-2 選択的阻害薬投与によって心筋梗塞や脳卒中の危険度が増加することが報告されているが，COX-2 の生理的働きには二面性があると考えられる(図 4)．それは既述したように，マクロファージ系細胞と血管内皮細胞で COX-2 の発現が異なった制御を受けることからも想定されるが，関連する知見として常在性マクロファージではプロスタサイクリン合成酵素と COX-2 が発現していること，応答性マクロファージでは COX-2 の発現が抑制されていること，活性化マクロファージでは COX-2 発現の増加とともに，トロンボキサン合成酵素の発現が強まることがあげられる[11]．また，血管内皮細胞において静脈血程度の弱い流れ刺激で COX-2 が誘導され，PGI_2産生に関与していること[12]，さらに強い流れ刺激を与えるとリポカリン型 PGD_2合成酵素が誘導され[13]，それによって合成された PGD_2代謝産物(15d-PGJ_2)が細胞保護作用，抗炎症作用，平滑筋増殖抑制作用に関与すると考えられる[14]．

15d-PGJ_2の問題点

尿中や培養液中における測定の結果，15d-PGJ_2は内因性リガンドではないとする報告がなされた[15]．さらに，15d-PGJ_2は親電子性化合物であることから，さまざまな蛋白質(IκB キナーゼ，Nrf2，チオレドキシン，チオレドキシン還元酵素，H-ras，プロテアソーム系，c-Jun など)との共有結合を介して作用することが報告されている[16]．15d-PGJ_2

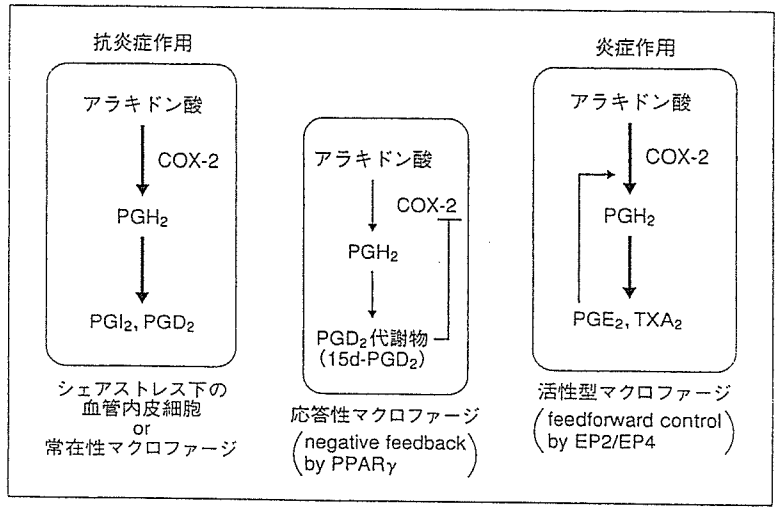

図 4　COX-2の二面性

のさまざまな生理作用を考慮すると，PPARγに依存しない，これらの作用機構も重要である．一方で，15d-PGJ_2が PPARγのリガンド結合部分に共有結合して働くことが報告された[17]．この場合，15d-PGJ_2の 13 位の炭素にリガンド結合ポケット内のシステイン残基が共有結合(マイケル付加反応)をしており，他の蛋白質で報告されている 9 位の炭素に蛋白質表面に露出したシステイン残基が共有結合する場合とは異なっていることが指摘されている．さらに，15d-PGJ_2の α,β-不飽和ケトン構造が PPARγ活性化に重要であり，この構造をもつ化合物が内因性リガンドとして働くこと，その作用は合成リガンドにおける活性化と異なっていることを報告している[17]．魅力的な提案であり，今後の検証が待たれる．

15d-PGJ_2は PGE_2の代謝産物である PGA_2とともに，以前より抗腫瘍活性，抗ウイルス活性，細胞周期の G_1停止活性が示されている．通常の PG には G 蛋白質共役型の細胞膜型受容体の存在が明らかになっているが，PGJ_2および PGA_2シリーズの PG には細胞膜型受容体が見出されておらず，核に移行することが知られていた．なお PGA_2をリガンドとする核内受容体として NR4A ファミリー(Nur77, Nurr1, NOR1)が報告されている[18]．また，細胞内で COX は小胞体と核膜の両方に検出される．したがって，15d-PGJ_2が PPARγの内因性リガンドとして働くことはこれらの知見と一貫性をもつように考えられるが，さらに検討をしていく必要がある．

植物ポリフェノール類

レスベラトロールは赤ワインに含まれる，抗酸化作用をもつフィトアレキシン(抗菌性物質)である．レスベラトロールは，中等度のワイン消費が心血管病，脳卒中，痴呆の危険度と負の相関を示す，いわゆる“フレンチパラドックス”に関与する物質と考えられてきた．著者らは，①レスベラトロールは核内受容体群のうち，PPARαおよび PPARγを選択的に活性化すること，②その活性化は血管内皮細胞およびニューロンで認められること，③レスベラトロールおよび PPARα リガンドを 3 日間経口投与後に，24 時間脳虚血にすると，脳梗塞の体積がコントロールに比べ有意に減少し，脳保護効果が認められること，④その脳保護効果は PPARα ノックアウトマウスでは認められないことを明らかにした．これらの結果から，レスベラトロールによる PPARαの活性化は“フレンチパラドックス”を説明する新しい作用機構を提供すると考えている[19]．

共同研究のなかで著者らは，レスベラトロールが COX-2 の発現を抑制することを以前に報告しているが[20]，それ以外の天然物質としてプロポリスに含まれるクリシン[21]，マンゴスチンに含まれるγ-マンゴスチン[22]も報告してきた．それ以外の

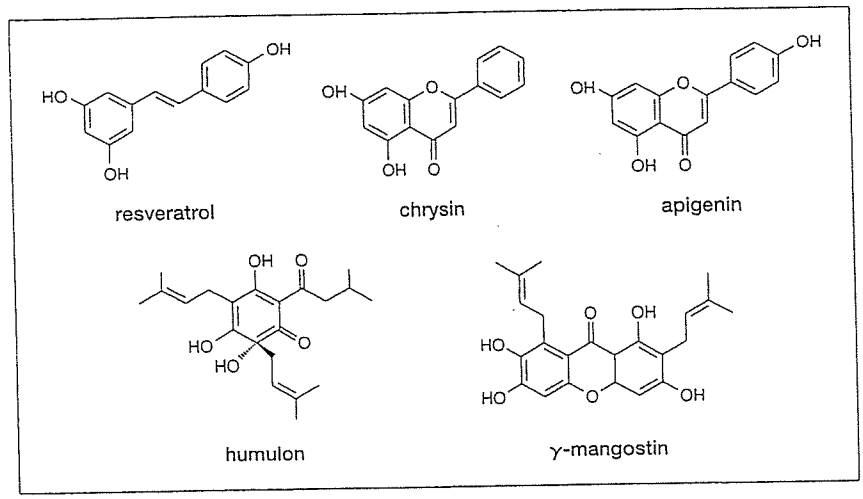

図 5　COX-2の発現を抑制する天然物質

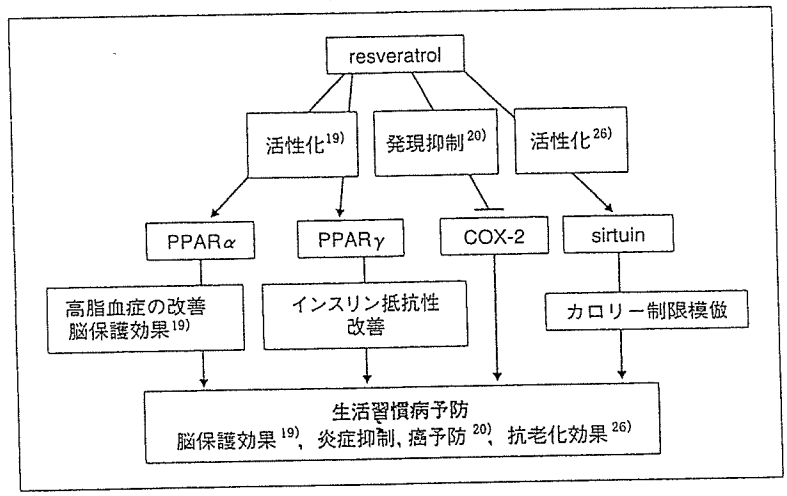

図 6　レスベラトロールのさまざまな作用

天然物質としてパセリに含まれるアピゲニン[23)]，ビールホップ成分であるフムロン[24)]が報告されている(図 5)．興味深いことに，γ-マンゴスチンを除いて，これらの物質はいずれも PPARα あるいはγのアゴニストとしても報告されている[23,25)]．著者らは現在，さまざまな植物ポリフェノールについて，PPAR 活性化能を指標にして検討を行っており，その構造と PPAR 活性化との関連，COX-2 発現抑制効果との関連を明らかにしていきたいと考えている．これらの研究は食による生活習慣病予防のエビデンスにつながっていくと期待している．

おわりに

以前よりカロリー制限はラットで老化を遅らせ，寿命を延長させることが知られている．そこでカロリー制限の機構を解明し，その効果のみを模倣する薬剤の開発が行われている．そのスクリーニングの結果，興味深いことにレスベラトロールが見出され，酵母の寿命をのばすことが報告された[26)]．その効果は NAD^+依存性脱アセチル化酵素 Sirtuin ファミリーの活性化に由来すると報告されたが，Sirtuin はさまざまな転写調節に関与しており，核内受容体とも相互作用していると考えられる．最近，DNA チップによる解析で，カ

ロリー制限を行ったネズミと核内受容体 PPARα のアゴニストを投与したネズミではよく似た遺伝子の発現パターンを示すことが報告され[27]，著者らも同様な結果をレスベラトロール投与で得ている(投稿準備中)．しかし一方で，レスベラトロールで活性化される Sirtuin は PPARγ の活性化を抑制することで，白色脂肪細胞において脂肪代謝を活性化するという報告もなされた[28]．この結果は，レスベラトロールが PPARγ も同時に活性化するという著者らの結果とは一致しない．

現在までの報告を単純に並列にまとめると図6のようになる．注目すべきことに，レスベラトロールに関して，さまざまな *in vivo* の効果を示す論文が多数報告されている[29,30]．したがって，PPAR, COX, Sirtuin がどのような関係にあるのかを明らかにすることは，生活習慣病予防の視点から今後の検討されるべき価値があると考えられる．

文献

1) 室田誠逸，山本尚三(編)：プロスタグランジン研究の新展開．東京化学同人，2001，pp.111-141.
2) Evans, R. M. et al. : *Nat. Med.*, **10** : 355-361, 2004.
3) Xu, M. E. et al. : *Proc. Natl. Acad. Sci. USA*, **98** : 13919-13924, 2001.
4) Forman, B. M. et al. : *Cell*, **83** : 803-812, 1995.
5) Kliewer, S. A. et al. : *Cell*, **83** : 813-819, 1995.
6) Inoue, H. et al. : *FEBS Lett.*, **350** : 51-54, 1994.
7) Inoue, H. et al. : *J. Biol. Chem.*, **270** : 24965-24971, 1995.
8) Inoue, H. et al. : *Biochem. Biophys. Res. Commun.*, **254** : 292-298, 1998.
9) Inoue, H. et al. : *J. Biol. Chem.*, **275** : 28028-28032, 2000.
10) 井上裕康：ビタミン，**77**：449-458，2003.
11) Kuwamoto, S. et al. : *FEBS Lett.*, **409** : 242-246, 1997.
12) Inoue, H. et al. : *Artherioscler. Thromb. Vasc. Biol.*, **22** : 1415-1420, 2002.
13) Taba, Y. et al. : *Circ. Res.*, **86** : 967-973, 2000.
14) Sasaguri, T. and Miwa, Y. : *Curr. Vasc. Pharmacol.*, **2** : 103-114, 2004.
15) Bell-Parikh, L. C. et al. : *J. Clin. Invest.*, **112** : 945-955, 2003.
16) 柴田貴広，内田浩二：生化学，**77**：1189-1192，2005.
17) Shiraki, T. et al. : *J. Biol. Chem.*, **280** : 14145-14153, 2005.
18) Kagaya, S. et al. : *Biol. Pharm. Bull.*, **28** : 1603-1607, 2005.
19) Inoue, H. et al. : *Neurosci. Lett.*, **352** : 203-206, 2003.
20) Subbaramaiah, K. et al. : *J. Biol. Chem.*, **273** : 21875-21882, 1998.
21) Woo, K. J. et al. : *FEBS Lett.*, **579** : 705-711, 2005.
22) Nakatani, K. et al. : *Mol. Pharmacol.*, **66** : 667-674, 2004.
23) Liang, Y. C. et al. : *FEBS Lett.*, **496** : 12-18, 2001.
24) Yamamoto, K. et al. : *FEBS Lett.*, **465** : 103-106, 2000.
25) Yajima, H. et al. : *J. Biol. Chem.*, **279** : 33456-33462, 2004.
26) Howitz, K. T. et al. : *Nature*, **425** : 191-196, 2003.
27) Corton, J. C. et al. : *J. Biol. Chem.*, **279** : 46204-46212, 2004.
28) Picard, F. et al. : *Nature*, **429** : 771-776, 2004.
29) Lastra, C. A. and Villegas, I. : *Mol. Nutr. Food Res.*, **49** : 405-430, 2005.
30) Baur, J. A. and Sinclair, D. A. : *Nat. Rev. Drug Discov.*, **5** : 493-506, 2006.

* * *

THE JOURNAL OF BIOLOGICAL CHEMISTRY VOL. 282, NO. 4, pp. 2741–2751, January 26, 2007

Solution Structure of the Cytoplasmic Region of Na^+/H^+ Exchanger 1 Complexed with Essential Cofactor Calcineurin B Homologous Protein 1*[S]

Received for publication, April 28, 2006, and in revised form, October 6, 2006 Published, JBC Papers in Press, October 18, 2006, DOI 10.1074/jbc.M604092200

Masaki Mishima[‡], Shigeo Wakabayashi[§], and Chojiro Kojima[‡1]

From the [‡]Graduate School of Biological Sciences, Nara Institute of Science and Technology, Ikoma, Nara 630-0192, Japan and [§]Department of Molecular Physiology, National Cardiovascular Center Research Institute, Suita, Osaka 565-8565, Japan

Na^+/H^+ exchanger 1 (NHE1) regulates intracellular pH, Na^+ content, and cell volume. Calcineurin B homologous protein 1 (CHP1) serves as an essential cofactor that facilitates NHE1 exchange activity under physiological conditions by direct binding to the cytoplasmic juxtamembrane region of NHE1. Here we describe the solution structure of the cytoplasmic juxtamembrane region of NHE1 complexed with CHP1. The region of NHE1 forms an amphipathic helix, which is induced by CHP1 binding, and CHP1 possesses a large hydrophobic cleft formed by EF-hand helices. The apolar side of the NHE1 helix participates in extensive hydrophobic interactions with the cleft of CHP1. We suggest that helix formation of the cytoplasmic region of NHE1 by CHP1 is a prerequisite for generating the active form of NHE1. The molecular recognition detailed in this study also provides novel insight into the target binding mechanism of EF-hand proteins.

Na^+/H^+ exchangers comprise a family of countertransport proteins that catalyze the electroneutral exchange of Na^+ and H^+. Nine isoforms of the Na^+/H^+ exchanger have been isolated and shown to possess similar membrane topologies consisting of 12 N-terminal membrane-spanning helices and a large C-terminal cytoplasmic region (Fig. 1*A*). The exchanger isoforms exhibit tissue-specific expression, membrane localization, and kinetic and pharmacological properties (1). They participate in a broad range of physiological processes including the regulation of cell volume, transepithelial transport of electrolytes, cell proliferation, apoptosis, and differentiation. Isoforms NHE1–5, localized at the plasma membrane, are primarily involved in the regulation of intracellular pH (pH_i)[2] and Na^+ concentration (1).

Of them, the ubiquitously expressed isoform NHE1 is the best studied mammalian Na^+/H^+ exchanger. The activity is controlled by various extrinsic factors including hormones, growth factors, pharmacological agents, and mechanical stimuli (1). The regulation of NHE1 by these external stimuli is thought to be exerted through the action of a variety of signaling molecules including calcineurin B homologous protein (2, 3), calmodulin (4, 5), low molecular mass GTPases of the Ras and Rho family (6–8), p42/44 mitogen-activated protein kinases (9), p90 ribosomal S6 kinase (10), 14-3-3 protein (11), Nck-interacting kinase (12), and phosphatidylinositol 4,5-bisphosphate (13). However, the detailed mechanism through which these events occur remains unknown.

Among these factors, CHP1 can serve as an essential cofactor and is required by at least three NHE isoforms (NHE1–3) to express high physiological levels of exchange activity (3). It was shown that CHP1 bound directly to the juxtamembrane region of the C-terminal cytoplasmic domain. When GFP-CHP1 and NHE1–3 were co-expressed, it was found that GFP-CHP1 was mostly localized at the cell surface, whereas co-expression of CHP1 and a CHP1 binding-defective NHE1 mutant failed to show co-localization, implying that NHE1 is a principal target of CHP1 (3). In addition to reduced activity in the neutral pH range, the CHP1 binding-defective NHE1 mutant showed a marked reduction in pH_i sensitivity (~0.7 pH unit acidic shift) that subsequently abolished various NHE1 regulatory responses. Furthermore CHP1 deprivation resulted in marked reduction (>90%) of NHE1 activity (3). These observations suggest that the association of NHE1 with CHP1 is critical for activity and the maintenance of NHE1 pH_i sensitivity (14).

CHP1 consists of four EF-hands, the primary sequence of which is homologous to calmodulin (CaM) and calcineurin B

* This work was supported in part by grants-in-aid for Scientific Research on Priority Area and the 21st Century of Excellence (COE) Program from the Ministry of Education, Culture, Sports, Science and Technology (MEXT), Japan (to M. M. and C. K.), and Grant nano-001 for Research on Advanced Medical Technology from the Ministry of Health, Labor and Welfare of Japan and Grant-in-aid for Priority Areas 13142210 for Scientific Research from the MEXT (to S. W.). The costs of publication of this article were defrayed in part by the payment of page charges. This article must therefore be hereby marked "*advertisement*" in accordance with 18 U.S.C. Section 1734 solely to indicate this fact.

[S] The on-line version of this article (available at http://www.jbc.org) contains supplemental Table S1 and Figs. S2 and S3.

The atomic coordinates and structure factors (code 2E30) have been deposited in the Protein Data Bank, Research Collaboratory for Structural Bioinformatics, Rutgers University, New Brunswick, NJ (http://www.rcsb.org/).

[1] To whom correspondence should be addressed: Graduate School of Biological Sciences, Nara Institute of Science and Technology, 8916-5 Takayama, Ikoma, Nara 630-0192, Japan. Tel.: 81-743-72-5571; Fax: 81-743-72-5579; E-mail: kojima@bs.naist.jp.

[2] The abbreviations used are: pH_i, intracellular pH; HSQC, heteronuclear single quantum coherence; NOE, nuclear Overhauser effect; NOESY, NOE spectroscopy; TOCSY, total correlation spectroscopy; CANDID, combined automated NOE assignment and structure determination module; CaM, calmodulin; CNB, calcineurin B; NHE, Na^+/H^+ exchanger; CHP, calcineurin B homologous protein; CNA, calcineurin A; Ni-NTA, nickel-nitrilotriacetic acid; GST, glutathione *S*-transferase; CHAPS, 3-[(3-cholamidopropyl)dimethylammonio]-1-propanesulfonic acid; r.m.s., root mean square; Kv, voltage-gated potassium channel; KChIP, Kv-interacting protein; PIP_2, phosphatidylinositol 4,5-bisphosphate.

Supplemental Material can be found at: http://www.jbc.org/cgi/content/full/M604092200/DC1

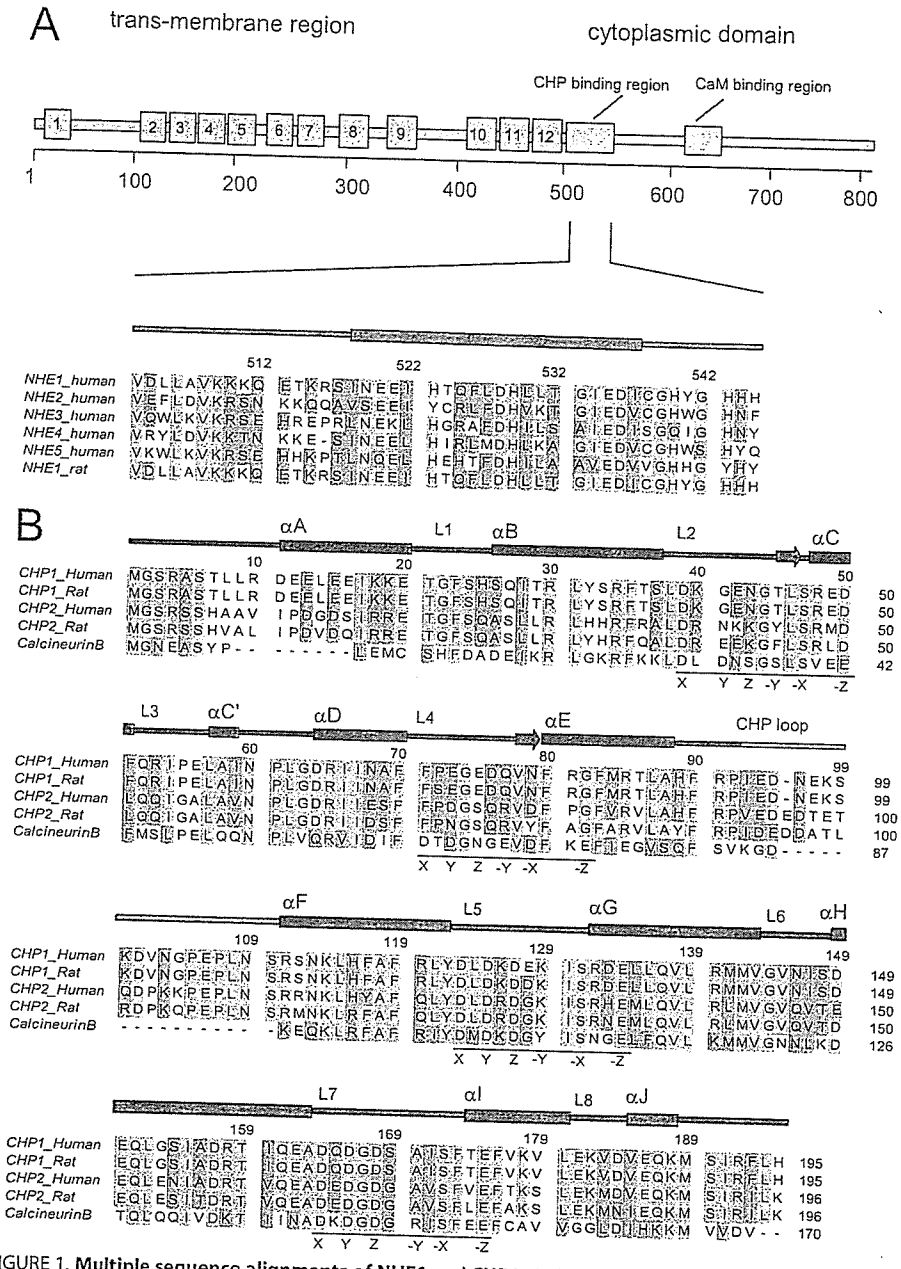

FIGURE 1. **Multiple sequence alignments of NHE1 and CHP1.** *A*, domain structure and alignment of NHE1. *B*, alignment of CHP1, CHP2, and human calcineurin B. In *A* and *B*, sequence alignment was performed using ClustalW. Secondary structure elements of the proteins are shown schematically at the *top* of the alignments. N- and C-terminal domains of CHP1 are colored in *blue* and *magenta*, respectively, for clarity. Conserved and semiconserved residues are colored in *yellow* and *green*, respectively. The 12-residue motif involved in the EF-hand is *underlined*, and key residues are indicated as *X*, *Y*, *Z*, *-Y*, *-X*, and *-Z*.

(CNB), possessing 31 and 41% sequence identity, respectively (Fig. 1*B*). It is well known that all CaM and CNB EF-hands can bind Ca^{2+}. However, CHP1 EF-1 and EF-2 are ancestral and do not bind Ca^{2+} under physiological conditions, whereas EF-3 and EF-4 bind two Ca^{2+} ions with high affinity (~90 nM) based on the $^{45}Ca^{2+}$ binding experiments for several CHP1 mutants (14). Complex formation between CHP1 and the CHP1 binding domain of NHE1 resulted in a marked increase in Ca^{2+} binding affinity (K_d = ~2 nM) (14). This suggests that CHP1 constitutively contains two Ca^{2+} ions when associated with NHE1 in cells (14).

Interestingly CHP1 has been reported to exhibit multiple functions. It was initially identified as a protein (p22) involved in vesicular transport (15) and the inhibition of calcineurin phosphatase activity (16). It was also found to interact with microtubules (17), DRAK2 (death-associated protein kinase-related apoptosis-inducing protein kinase 2) (18) and KIF1Bβ2 (kinesin family 1Bβ2) (19).

A second CHP isoform, CHP2, with 61% sequence identity was also identified and found to be involved in the maintenance of abnormally high pH_i in malignantly transformed cells. CHP2 is expressed at a relatively high level in malignantly transformed cells and in rat small intestine, suggesting that it plays a specific role in this tissue (20). In addition, tescalcin, an EF-hand protein closely related to CNB, that interacts with the cytoplasmic region of NHE1 has been identified (21, 22).

The crystal structure of NHE1-unbound rat CHP1 was recently determined and revealed that the overall structure is similar to CNB where Ca^{2+} ions are coordinated within EF-3 and EF-4. However, the interaction mechanism between NHE1 and CHP1 remains unknown (23).

Here we report on the solution structure of the cytoplasmic region of NHE1 bound to CHP1 as determined by NMR. Details of the NHE1-CHP1 interaction are described. We present mutational binding data to delineate the significance of the interactions observed in the complex. Based on the structure, we suggest a role for CHP1 in terms of NHE1 activation. Comparisons of the binding mode between NHE1-CHP1 and calcineurin A (CNA), CNB, and other related four-EF-hand proteins are also discussed.

EXPERIMENTAL PROCEDURES

Sample Preparation—The NHE1-CHP1 complex was co-expressed and co-purified. DNA encoding NHE1 was cloned into the pET24a vector (Novagen), and CHP1 was subcloned into pET11a (Novagen), which produces recombinant protein with a hexahistidine (His_6) sequence at the C terminus. The proteins were co-overexpressed in *Escherichia coli* BL21(DE3) cells. Uniformly ^{15}N- and $^{15}N/^{13}C$-labeled proteins were prepared by

growing bacteria in minimal medium containing $^{15}NH_4Cl$ with or without [$^{13}C_6$]glucose. Uniformly $^{15}N/^{13}C$-labeled and fractionally deuterated protein sample was prepared using medium containing 60% ^2H_2O. The NHE1-CHP1 complex was purified using a standard Ni-NTA affinity column protocol (Qiagen). Further purification was performed by gel filtration using Superdex 200 (GE Healthcare). NMR samples contained 0.5–0.9 mM protein in 50 mM Tris-d_7 buffer (pH 6.9), 1 mM dithiothreitol-d_{10}, 30 mM KCl in $H_2O/^2H_2O$ (9:1) or ^2H_2O.

NMR Spectroscopy—NMR data were recorded at 37 °C on Bruker AVANCE 500 and DRX 800 NMR spectrometers. Resonance assignments for ^{1}HN, ^{15}N, $^{13}C\alpha$, $^{13}C\beta$, and $^{13}C'$ nuclei for the CHP1-NHE1 complex were obtained through the following ^{2}H-decoupled, triple resonance spectra applied to a fractionally deuterated $^{15}N/^{13}C$-labeled sample: three-dimensional HNCACB/HN(CO)CACB (24) and three-dimensional HN(CA)CO/HNCO experiments (25, 26). Side-chain ^{1}H and ^{13}C resonances were assigned on a fully protonated sample or a fractionally deuterated $^{15}N/^{13}C$-labeled sample using three-dimensional C(CO)NH, three-dimensional H(CCO)NH, four-dimensional HC(CO)NH, and three-dimensional HCCH TOCSY (27–29). Stereospecific assignment of leucine and valine methyl groups were obtained from a Constant Time-$^1H/^{13}C$ HSQC spectrum of a 15% ^{13}C-labeled sample (30). $^1H\alpha$ and $^1H\beta$ resonance assignments were supplemented with three-dimensional H(CACO)NH (31), ^{15}N-edited TOCSY-HSQC (32), and three-dimensional HBHA(CBCACO)NH (33). Aromatic resonances of both NHE1 and CHP1 were mainly assigned using three-dimensional ^{13}C-aromatic-edited/^{15}N-separated NOESY-HSQC, three-dimensional ^{13}C-edited NOESY, ^1H-^1H TOCSY, and NOESY experiments (32). The assignment was verified using the Constant Time-$^1H/^{13}C$ HSQC spectrum of a 15% ^{13}C-labeled sample (30). The following NOESY spectra were recorded for the protonated sample and used to generate distance restraints for structure calculations: three-dimensional ^{15}N-edited NOESY (80-ms mixing time), three-dimensional ^{13}C-edited NOESY (80-ms mixing time), and two-dimensional ^{1}H NOESY (80-ms mixing time). Slowly exchanging amide protons were identified from a series of two-dimensional ^{15}N HSQC spectra recorded after the H_2O buffer was replaced with ^2H_2O buffer. All NMR spectra were processed using NMRPipe/NMRDraw (34) analyzed using SPARKY (35).

Structure Calculations—Intramolecular and intermolecular distance constraints were identified in the three-dimensional $^{15}N/^{13}C$-separated NOESY spectra using a $^{15}N/^{13}C$-labeled NHE1-CHP sample with mixing times of 80 ms. Backbone hydrogen bond restraints within regular secondary structure elements that were consistent with backbone amide hydrogen/deuterium exchange data were included in the structure calculations. The initial structure calculations were performed by iterative automated assignment of the NOE spectra using CANDID (36) in addition to manually assigned NOE-derived distance restraints. The restraints, leading to converged structures, were subsequently utilized for the iterative automated assignment of all spectra including aromatic residues using CANDID. Finally refinement of the structures (including two Ca^{2+} ions) using XPLOR-NIH (version 2.96) was performed (37). The final structure calculations used a total of 4022 NOE-derived distance restraints obtained from the manual and the CANDID-assisted assignments from the ^{15}N- or ^{13}C-edited NOE data. A total of 100 simulated annealing structures were calculated, and 20 structures were selected that possessed no NOE violations greater than 0.5 Å and no dihedral violations greater than 5°. Final structures were evaluated using the program ProcheckNMR (38). Structures and figures were drawn using MOLMOL (39), GRASP (40), and Chimera (41).

Mutagenesis and GST Pulldown Assay—For the binding analyses, CHP1 was expressed as a fusion protein with GST in *E. coli*, which was then subcloned into modified pGEX6P-3 (Novagen) (42). Site-directed mutant proteins were prepared using the QuikChange kit (Stratagene). DNA sequencing confirmed the mutations. Vectors were transformed into BL21(DE3)star (Invitrogen). Cells were grown at 37 °C and then induced with 1 mM isopropyl 1-thio-β-D-galactopyranoside for 12 h at 20 °C. Harvested cells were disrupted via sonication in HEPES (pH 8.0) containing 10% glycerol, 10% sucrose, 1 mM dithiothreitol, and 30 mM KCl. The GST-CHP1 fusion protein was purified using glutathione-Sepharose (GE Healthcare) and a standard protocol except that the equilibrium buffer was changed to 50 mM HEPES buffer (pH 8.0) containing 10% glycerol, 1 mM dithiothreitol, and 30 mM KCl, and the column was washed extensively with 20 mM CHAPS. The effect of mutation on the binding of CHP1 to NHE1 peptides was characterized using a GST pulldown assay. Synthetic NHE1 peptide (residues 514–545 including a hexahistidine sequence at the C terminus) was purchased from Greiner Japan (Tokyo, Japan). Briefly wild-type and CHP1 mutant GST fusion proteins, in addition to GST alone, were incubated for 30 min at 20 °C with NHE1 peptide in binding buffer containing 50 mM HEPES (pH 7.5), 20 mM CHAPS, 10% glycerol, 1 mM Pefabloc, and 1 mM dithiothreitol. GST protein-bound Sepharose beads were washed extensively with binding buffer. Proteins were resolved by 12% NuPAGE (Invitrogen) and blotted onto membranes, and then His-NHE1 was analyzed with Ni-NTA-conjugated alkaline phosphatase (Promega) and Western Blue substrate (Promega). Quantification was represented as the average value of experiments performed in triplicate.

RESULTS AND DISCUSSION

Structure Determination—To better understand the mechanism pertaining to CHP1-regulated NHE1 activity, the solution structure of unmyristoylated CHP1 complexed with the cytoplasmic region (503–545) of NHE1 was determined by NMR spectroscopy. Our structural studies were initially hampered by the fact that NHE1-free CHP1 tended to aggregate during NMR measurements, and the CHP1-unbound cytoplasmic region (503–545) of NHE1 readily degraded during the expression and purification steps. Consequently NMR structural analysis of co-expressed and co-purified samples was undertaken. Co-expression of CHP1 and NHE1-(503–545) produced a stable complex for structural studies and showed no significant degradation and aggregation for several weeks.

The ^1H-^{15}N HSQC spectrum of NHE1-unbound CHP1 displays many broadened peaks presumably due to formation of a dimer, multimer, or an equilibrium between these states in solution. In contrast, the HSQC spectrum of ^{15}N-labeled CHP1